Original article

MOLECULAR METABOLISM

Tumoral acidosis promotes adipose tissue depletion by fostering adipocyte lipolysis

Camille Lefevre[1,], Morgane M. Thibaut[1], Audrey Loumaye[2,3], Jean-Paul Thissen[2,3], Audrey M. Neyrinck[1], Benoit Navez[5], Nathalie M. Delzenne[1], Olivier Feron[4,6], Laure B. Bindels[1,6,*]**

ABSTRACT

Objective: Tumour progression drives profound alterations in host metabolism, such as adipose tissue depletion, an early event of cancer cachexia. As fatty acid consumption by cancer cells increases upon acidosis of the tumour microenvironment, we reasoned that fatty acids derived from distant adipose lipolysis may sustain tumour fatty acid craving, leading to the adipose tissue loss observed in cancer cachexia.
Methods: To evaluate the pro-lipolytic capacities of acid-exposed cancer cells, primary mouse adipocytes from subcutaneous and visceral adipose tissue were exposed to pH-matched conditioned medium from human and murine acid-exposed cancer cells (pH 6.5), compared to naive cancer cells (pH 7.4). To further address the role of tumoral acidosis on adipose tissue loss, a pH-low insertion peptide was injected into tumour-bearing mice, and tumoral acidosis was neutralised with a sodium bicarbonate buffer. Prolipolytic mediators were identified by transcriptomic approaches and validated on murine and human adipocytes.
Results: Here, we reveal that acid-exposed cancer cells promote lipolysis from subcutaneous and visceral adipocytes and that dampening acidosis *in vivo* inhibits adipose tissue depletion. We further found a set of well-known prolipolytic factors enhanced upon acidosis adaptation and unravelled a role for β-glucuronidase (GUSB) as a promising new actor in adipocyte lipolysis.
Conclusions: Tumoral acidosis promotes the mobilization of fatty acids derived from adipocytes *via* the release of soluble factors by cancer cells. Our work paves the way for therapeutic approaches aimed at tackling cachexia by targeting the tumour acidic compartment.

Keywords Tumor acidosis; Adipose tissue; Lipolysis; Adipocytes; Cancer cachexia; Beta-glucuronidase

1. INTRODUCTION

Tumoral acidosis, as a tumour microenvironment hallmark [1], is an adaptative feature of rapid growth and proliferation of cancer cells [1,2]. The high energy demand provided by glycolysis and CO_2 hydration supports acidosis by producing lactate and H^+ ions. Acidosis is also maintained by poor tissue perfusion [1,2]. The extracellular pH of solid tumours (ranging mostly from 6.5 to 7.0) is lower than the extracellular pH of normal tissues (~7.4) [1] and contributes to tumour progression by promoting proliferation, invasion, evasion of apoptosis, and immune surveillance, thereby conferring resistance to chemo- and radio-therapies [1,2].
This tumoral acidosis drives a metabolic reprogramming of cancer cells towards fatty acid mobilization, supporting tumour progression and metastasis [3–5]. In acid-exposed cancer cells, glucose oxidation decreases in favor of fatty acids, and glutamine to a lesser extent [3]. This fatty acid metabolism shift is driven by an increase in the uptake of fatty acids that are either stored as triglycerides in lipid droplets or oxidized to generate ATP to fulfil immediate cellular needs [3–5]. Targeting the fatty acid metabolism with etomoxir, an inhibitor of carnitine palmitoyl transferase CPT1, limits the *in vivo* tumoral growth of cancer cells pre-exposed to acidosis [3] and inhibits the development of lung metastasis in mice injected intravenously with pH6.5-exposed cancer cells [5].
The increased availability of fatty acids appears to increase fatty acid storage and oxidation within cancer cells in parallel with their invasive potential [6]. Along these lines, peritumoral adipocytes support tumour proliferation, invasion, and migration, as shown by adipocyte-cancer cell cocultures [7–9]. Recently, Deroanne's team highlighted that in breast cancer extracellular tumoral acidosis promotes lipolysis in cancer-associated adipocytes [10]. Nevertheless, the role of this tumoral acidosis in fatty acid mobilization from distant adipose tissues, and thereby adipose tissue depletion, is not known.
Such adipose tissue depletion is part of the cachexia syndrome [11]. 60–80% of patients with advanced cancer experience cancer cachexia, a wasting syndrome associated with involuntary weight loss consecutive to muscle mass and adipose tissue depletion. Cancer cachexia limits both survival and anticancer response in patients and is

[1]Metabolism and Nutrition Research Group, Louvain Drug Research Institute, UCLouvain, Université catholique de Louvain, Brussels, Belgium [2]Department of Endocrinology and Nutrition, Cliniques Universitaires Saint-Luc, Brussels, Belgium [3]Department of Endocrinology, Diabetology and Nutrition, IREC, UCLouvain, Brussels, Belgium [4]Pole of Pharmacology and Therapeutics (FATH), Institut de Recherche Expérimentale et Clinique (IREC), UCLouvain, Brussels, Belgium [5]Department of Abdominal Surgery and Transplantation, Cliniques universitaires Saint-Luc, Brussels, Belgium [6]Welbio Department, WEL Research Institute, Wavre, Belgium

*Corresponding author. Avenue E. Mounier, 73, B1.73.11, 1200 Brussels, Belgium. Tel.: +32 2 764 73 37. E-mail: laure.bindels@uclouvain.be (L.B. Bindels).

**Corresponding author. E-mail: ca.lefevre@uclouvain.be (C. Lefevre).

Received January 15, 2024 • Revision received March 20, 2024 • Accepted March 28, 2024 • Available online 1 April 2024

https://doi.org/10.1016/j.molmet.2024.101930

Abbreviations

ADM	adrenomedullin
ANOVA	Analysis of variance
ATGL	Adipose triglyceride lipase
BMI	Body weight index
BSA	Bovine serum albumin
C	Cachectic
C4A/B	Complements C4A/B
CA2	Carbonic Anhydrase 2
CD36	Cluster of differentiation 36
CPT1	Carnitine palmitoyl transferase 1
CGI-58	Comparative gene identification-58 protein
DMEM	Differentiation medium, basal medium
DPP7	Dipeptidyl Peptidase 7
EAT	Epididymal adipose tissue
FBS	Fetal bovine serum
FABP4	Fatty acid binding protein 4
FASN	Fatty acid synthase
FSP27	Fat-specific protein 27
G0S2	G0/G1 switch 2
GUSB	β-glucuronidase
HPRT	Hypoxanthine guanine phosphoribosyl transferase
HSL	Hormone-sensitive lipase
pHSL	Phosphorylated HSL
IL6	Interleukin 6
Iso	Isoproterenol
IBMX	Isobuthylmethylxanthine
LAL	Lysosomal acid lipase
LAMP2	Lysosomal associated membrane protein 2
Lipa	Lipase A, Lysosomal acid type
MAT	Mesenteric adipose tissue
MCT4	Monocarboxylate transporter 4
MDSEC	Majority decision-based method for secreted proteins
MGL	Monoacylglycerol lipase
NC	Non-cachectic
NEFA	non-esterified fatty acids
LAMA1	Laminin Subunit Alpha 1
LFC	Log 2 fold change
OAZ1	Ornithine decarboxylase antizyme 1
PCA	Principal Component Analysis
PERMANOVA	Permutational analysis of variance
pH6.5/cancer cells	Acid-exposed cancer cells
pH7.4/cancer cells	Naive cells maintained at pH7.4
pHLIP	pH-low insertion peptide
PLIN2	Perilipin2
PTHLH	Tumour-derived parathyroid hormone like hormone
PRDM16	PR/SET domain 16
PRL2C	Prolactin family 2, subfamily c
RPL6/19/27	Ribosomal protein L6/19/27
SAT	Subcutaneous adipose tissue
Ser	Serine
t0	time 0, at the beginning of incubation
TD-NMR	Nuclear magnetic resonance
TGFβ2	Transforming growth factor Beta 2
TNFα	Tumor necrosis factor alpha
TNFRSF1B	TNF Receptor Superfamily Member 1B active protein
Var3	variant 3
VAT	Visceral adipose tissue
ZAG	Zinc-alpha2-glycoprotein

responsible for at least 20% of cancer death [11,12]. Adipose tissue depletion is an early event in cancer cachexia [13]. Adipose tissue depletion often precedes muscle wasting [14,15] and preserving adipose tissue mass protects against muscle loss [16]. Moreover, fat depletion alone is sufficient to reduce the survival of patients and affect their anticancer response [14,17].

White adipose tissue stores energy in the form of lipids (*via* triglyceride synthesis, *de novo* lipogenesis, and adipogenesis) and releases free fatty acids through lipolysis [18]. Lipolysis mobilizes fatty acids from adipocytes through three lipases sequentially: adipose triglyceride lipase (ATGL), hormone-sensitive lipase (HSL), and monoacylglycerol lipase (MGL), with the first two being the rate-limiting enzymes. Lipolysis is a key process involved in the fat mass loss associated with cancer cachexia [19]. Cachectic adipocytes display increased basal and catecholamine-stimulated lipolysis [19—21]. Concordantly, several clinical and preclinical studies have reported an increase in HSL, its active form, phosphorylated HSL (pHSL), and ATGL [20—22]. In mice, genetic deletion of HSL or ATGL protects against tumour-induced fat mass loss and muscle atrophy [16]. Increased lipolysis was also associated with an increase in *de novo* lipogenesis, thereby feeding a futile cycle [22]. Proinflammatory mediators and tumour-derived prolipolytic factors drive these changes in adipose tissue [12]. Several prolipolytic mediators have been proposed, such as the tumour-derived parathyroid hormone like hormone (PTHLH), adrenomedullin (ADM), zinc-α2-glycoprotein (ZAG), proliferin-1, tumor necrosis factor alpha (TNFα) and interleukin 6 (IL6) [11,19,23]. Nevertheless, therapeutic targeting of key proinflammatory factors has not yielded meaningful improvements in cachexia management [24] while less conventional mediators (e.g. PTHLH, adrenomedullin and proliferin-1) were identified only in specific cancer types.

To our knowledge, the role of tumoral acidosis in adipose tissue depletion at distance from the tumour has not yet been investigated. A better understanding of the cooperation between the tumour microenvironment and macroenvironment (tumour—host interactions) could be crucial in the development of efficient treatments against cancer cachexia [24]. As fatty acid consumption by cancer cells increases upon acidosis adaptation, we reasoned that fatty acids derived from adipose tissue lipolysis could sustain tumour fatty acid craving, leading to the adipose tissue depletion observed in cancer cachexia. We further hypothesised that acid-exposed cancer cells foster lipolysis by releasing prolipolytic soluble factors that reach distant adipose tissues through the blood stream.

2. METHODS

2.1. Cell culture

Human colon HCT116, hypopharyngeal FaDu, cervix SiHa, pancreatic MIA PaCa-2 and PANC-1 cell lines, and murine colon C26 (from Dr Mario Colombo, Istituto Nazionale Tumori, Italy) and Lewis lung LLC (from Pierre Sonveaux, UCLouvain, Brussels, Belgium) carcinoma cells were maintained in DMEM (Sigma, D5030), 10% fetal bovine serum (FBS, Biowest, South America, S181B-050), 10 mM D-glucose, 2 mM L-glutamine, 100 Units/ml penicillin, 100 μg/ml streptomycin, buffered with 25 mM HEPES and 25 mM PIPES with pH adjusted to 7.4 or 6.5 [25]. Acid-exposed cancer cells (pH6.5/cancer cells) were *in vitro* exposed to pH6.5 for a minimum of 1 month before their use and

compared to naive cells maintained at pH7.4 (pH7.4/cancer cells). The 3T3-L1 (CL-173) cell line was purchased from ATCC. 3T3-L1 cells were maintained in basal medium (DMEM, 10% FBS (Biowest, South America, S181B-050), 25 mM D-glucose, 4 mM L-glutamine, 1 mM pyruvate, 100 Units/ml penicillin, 100 μg/ml streptomycin)) and did not exceed 70—80% confluence to maintain undifferentiated 3T3-L1. After collection, cell number was assessed by cell counting using blue trypan exclusion. All cells were maintained at 37 °C, 5% CO_2.

2.2. For conditioned medium preparation

pH6.5/ and pH7.4/cancer cells were plated to reach 80% confluence in 24 h, then maintained for 48 h in pH adjusted DMEM with 2% fatty acid-free bovine serum albumin (BSA, Sigma) replacing FBS. Control medium was deposited in wells without cells. The conditioned and control media were collected, spun for 5 min at 500 g to remove suspended cells, and buffered at pH 7.4.

2.3. Isolation of primary human and murine adipocytes

Patients were recruited after signature of the full consent form between November 2022 and August 2023. The clinical study TULIP (ClinicalTrials.gov ID: NCT05128318) was conducted in the service of abdominal surgery and transplants at Cliniques Universitaires Saint-Luc/Université Catholique de Louvain (Belgium), revised and approved in December 2021 by the University-hospital Ethic committee Saint-Luc-UCL. Inclusion criteria were as follows: 18—60 years old, who required abdominal surgery for Nissen fondoplicature or cholecystectomy, with a body weight index (BMI) between 18.5 and 30 kg/m^2. Exclusion criteria were patients non-caucasian with cancer, infection, metabolic syndrome, autoimmune or inflammatory diseases, patients with beta blocker, hypoglycaemic, anti-diabetic and/or lipid-lowering treatments. 1—2 cm^2 deep abdominal subcutaneous and grand epiploon visceral adipose tissues were harvested from patients. Patient characteristics are described in Table S1.

Mouse subcutaneous (SAT) and mesenteric adipose tissues (MAT) were harvested from 8 to 12 weeks old male C57BL/6J mice (Janvier, France) killed by cervical dislocation. Lymph nodes were removed from adipose tissues. Each isolation required SAT and MAT pools (1,5-2 g) from 6 mice to provide enough adipocytes.

Adipose tissues were collected and left on ice in DMEM 5,55 mM D-glucose, 4 mM L-glutamine, 100 Units/ml penicillin, 100 μg/ml streptomycin until adipocyte isolation. Adipose tissues were washed with PBS before being torn into pieces. Pieces were incubated for 30—35 min at 37 °C under agitation (220 rpm) in digestion buffer containing Krebs (120 mM NaCl, 6 mM KCl, 1,2 mM KH_2PO_4, $MgSO_4$), 2,5 mM CaCl2, 25 mM $NaHCO_3$, 5 mM D-glucose, 4% fatty acid-free bovine serum albumin (BSA, Sigma), 30 mM HEPES and 2 mg/mL Type I collagenase (ThermoFisher), pH 7.4. The digestion was stopped with 5 mM EDTA. Digested adipose tissues were filtered using 250 μm Pierce™ Tissue Strainers (ThermoFischer, Belgium) and spun for 1 min at 150 g at room temperature. The adipocyte fraction in suspension was isolated and washed twice in Krebs buffer, pH 7.4, 1.2 mM $CaCl_2$, 25 mM $NaHCO_3$, 30 mM HEPES and 2% fatty acid-free BSA, and spun 1 min at 150 g at room temperature.

2.4. Ex-vivo lipolysis on primary human and murine adipocytes

Isolated adipocytes were suspended in Krebs buffer, pH7.4, 1.2 mM $CaCl_2$, 25 mM $NaHCO_3$, 30 mM HEPES and 4 % fatty acid-free BSA at 30 000 adipocytes per 200 μl. 200 μl adipocytes in suspension and 200 μl 2% fatty acid-free conditioned medium were deposed in a ratio 1:1 in 48 well plates (Greiner). For control wells, isolated adipocyte suspension and control medium were deposited at a ratio 1:1 with or without 10 μM isoproterenol (Iso, Sigma), a β-adrenergic agonist, or with human recombinant glucuronidase beta (GUSB, Abcam, ab219458, Belgium). Control medium wells, with lipolysis buffer and control medium in ratio 1:1, were also prepared. Each condition was tested in triplicate. Supernatants from control wells were collected at the beginning of incubation (t0). Lipolysis occurred for 24—48 h under 250 rpm orbital agitation in a humidified 5% CO_2 atmosphere at 37 °C. Lipolytic activity of primary adipocytes was estimated as the concentration of glycerol in supernatants collected at 24 h and 48 h. The concentrations of glycerol at t0 and in the control medium were subtracted from the concentrations measured under each condition. Concentrations in control wells without Iso were then deducted from the concentrations measured in each condition before normalization to the number of cancer cells used to produce 200 μl of conditioned medium (mM per 10^5 cancer cells). The previously deducted concentrations in control well without Iso were then re-added to this normalised concentration.

2.5. 3T3-L1 differentiation into adipocytes and lipolysis

To induce differentiation, the 3T3-L1 fibroblast cell line was maintained for 2 days at confluence and then induced to differentiate into adipocytes with basal medium supplemented with 10 μg/ml human insulin (Actarapid, Novonordisk), 0.5 mM isobuthylmethylxanthine (IBMX), 0.5 μM dexamethasone, 2 nM T3, 2 μM rosiglitazone. Two days later, medium was changed to basal medium supplemented with 10 μg/ml human insulin for 48 h. Then medium was changed for 7 days with non-supplemented basal medium, refreshed every 2 days. At day 13 post-induction of differentiation, the adipocytes were exposed 6h—24 h to basal medium with 3% fatty acid-free BSA replacing FBS with Human recombinant proteins, β-glucuronidase (GUSB), complements C4A and C4B (Complement Technology, A106 and A108, USA), TNF Receptor Superfamily Member 1B active protein (TNFRSF1B, MyBiosources, MBS650291, USA), Dipeptidyl Peptidase 7 (DPP7, Biotechne, 3438-SE, USA) and Laminin Subunit Alpha 1 (LAMA1, MyBiosources, MBS2009836). Control wells with or without 1 μM Iso were included. The release of glycerol, representative of lipolysis, was normalised to protein levels. For protein extraction, 3T3L1 cells were suspended in RIPA buffer containing phosphatase and protease inhibitors, incubated for 1 h on ice, homogenized by vortexing every 20 min and centrifuged (15 min 20 000 g 4 °C). Protein supernatant collection and protein concentration measurement are described in the western-blot section.

2.6. Mouse experiments

All mouse experiments were approved by the UCLouvain ethical committee (approval IDs, and dates of approval: 2021/UCL/MD/046, July 2021, A5/UCL/MD/2022, April 2022; 2023/UCL/MD/A9, June 2023; 2023/UCL/MD/48, August 2023).

Male C57BL/6J and Rj:NMRI-Fxn1 nu/nu mice (6 and 7 weeks old, respectively, Janvier, France) were kept in specific pathogen-free conditions and housed in individually ventilated cages with a 12 h light/dark cycle and fed an irradiated chow diet (A04-10, Safe, France). Enrichment was insured through the furniture of nesting material and shelter.

After a one-week acclimatization, mice were randomly assigned to experimental groups based on their body weight. CT group (sham-injected) and tumour-bearing mice were subcutaneously injected with PBS vehicle, HCT116 or FaDu cancer cells (2×10^6 cells in 0.1 ml PBS) respectively in right anterior flank. Body weight, fat and lean mass, tumour size, food and water intake were monitored. Nuclear magnetic resonance (TD-NMR, minispec mq_{one}, Bruker) was

performed for fat and lean mass follow-up. Tumour volume (V) was calculated following formula $V = x \times x \times y \times 0.5$ (x, shortest diameter; y, longest diameter; measured using an electronic caliper (VWR)). Once tumour-injected, mice were monitored daily for signs of stress and anxiety, based on their physical condition and appearance, as well as their behaviour using a scoring grid. For these models, the humane endpoints were as follows: loss of 20% of the initial body weight; prolonged score (>24 h) greater than 3 or score superior to 5; tumour ulcerations; tumour volume exceeding 2000 mm^3.

In the acidosis neutralisation experiment, mice were divided into 3 groups (Figure 6D): CT group, HCT116-injected group and HCT116-$NaHCO_3$ (HCT116-injected mice treated *ad libitum* with 200 mM sodium bicarbonate (Qualiphar) in drinking water). $NaHCO_3$ treatment started 4 days post HCT116-injection until necropsy.

40 μM pHLIP(variant3) (var3: NH2-ACDDQNPWRAYLDLLFP-TDTLLLDLLW-COOH-AF568; Europeptide Thermofisher) in PBS, a pH-low insertion peptide targeting the tumoral acidosis [26], was injected i.v. 4–6 h before tumour resection [5]. Tumours were embedded in OCT, frozen in cold isopentane and maintained at −80 °C. Hoechst (2 μg/ml in PBS, H1399, Sigma) nuclear staining was carried out on acetone-fixed 5 μm tumour sections. Images were acquired using a slide scanner (Axioscan.z1, Zeiss). The percentage of cells positive for pHLIP was quantified using QuPath-0.3.2. To take tumour size into account, we calculated a pHLIP score according to the following formula: pHLIP score = cells positive for pHLIP (%) * tumour weight (g).

Blood samples from vena cava were harvested following anesthesia (isoflurane gas, Abbot, Belgium). In $NaHCO_3$ experiment, the blood pH was measured with a micro pH electrode adapted to volumes less than 100 μl (Hanna instruments) before separation of plasma. Following SAT (right anterior, left anterior and posterior) and visceral MAT and epididymal (EAT) adipose tissue collections. Tissues (after subcutaneous and mesenteric lymph nodes removal) were weighed and frozen in liquid nitrogen. All samples were stored at −80 °C until further analyses.

2.7. Cancer cell mRNA sequencing and tissue mRNA analyses

RNA samples from 3 human pH6.5/and pH7.4/cancer cell lines (HCT116, SiHa and FaDu) used for conditioned medium preparation, i.e. in 2% fatty acid-free BSA medium for 2 days, were sequenced after polyA selection using a 2 × 150 paired-end configuration 1.5 on an Illumina NovaSeq 6000 instrument (Genewiz, Germany). Raw sequence data generated were processed using Illumina's bcl2fastq 2.20 software. Raw fastq files were analysed *in house* as described previously [27]: briefly sequences were quality-controlled using FastQC (https://www.bioinformatics.babraham.ac.uk/projects/fastqc/) and trimmed by Trimmomatic version 0.38 [28]. Sequence reads were aligned to the annotated reference genome of *Homo sapiens* GRCh37.75 using STAR version 2.6.1d [29] and count matrices were generated from reads aligned to the reference genome using the function *summarizedOverlaps* from the R package *GenomicAlignments* version 1.36.0 [30]. Data were tested for differential expression and normalised using the R package *DESeq2* version 1.40.2 [31]. Raw RNA sequences can be found in the Gene Expression Omnibus (GEO) database (project ID: GSE253054).

To identify potential prolipolytic proteins mobilised under chronic acidosis adaptation, a list of genes per cancer cell line was extracted with p-adj <0.05 and a log 2 fold change (LFC) > ± 0.3. These genes were merged into a list of secreted proteins predicted by a majority decision-based method for secreted proteins (MDSEC) downloaded in February 2022 from "The Human Protein Atlas" library (Human Protein Atlas proteinatlas.org) [32,33]. The MDSEC list was constructed based on 3 peptide signal prediction methods: SignalIP, Phobius, Spoctopus [34]. All proteins predicted to be secreted by at least 2 methods were considered as "predicted secreted proteins". This method excludes genes that are predicted to reside in intracellular locations, such as endoplasmic reticulum or Golgi, despite having a signal peptide prediction. Venn diagrams (https://bioinformatics.psb.ugent.be/webtools/Venn/) were generated from these lists. PCA and PERMANOVA analyses were performed using the R package *MixOmics* version 6.24.0 [35]. The fold change in the expression of the genes encoding the predicted secreted proteins shared by the 3 cancer cell lines was correlated with the fold change in glycerol release from pH6.5/cancer cells on pH7.4/cancer cells using Spearman's correlation with R package Hmisc version 5.1–1.

Gene set enrichment analysis was conducted using clusterProfiler version 4.8.3 [36], fgsea version 1.26.0 [37] and goseq version 1.52.0 [38] on all expressed genes ranked by log 2 fold change. We used the gene set KEGG pathways databases as reference. Genes were mapped and coloured according to their padj and log 2 fold change.

Total RNA was isolated from tissues or cells using TriPure reagent (Roche, Basel, Switzerland). cDNA was prepared by reverse transcription of 1 μg total RNA using the Goscript RT Mix OligoDT kit (Promega, Leiden, Netherlands). Real-time polymerase chain reactions (PCR) were performed with a StepOnePlus/QuantStudio Real-Time PCR System and software (Applied Biosystems, Den Ijssel, The Netherlands) or a CFX96 TouchTM instrument and software (Bio-Rad Laboratories, CA, USA) using SYBR Green (GoTaq qPCR mix, Promega, USA) for detection. All samples were run in duplicate in a single 96-well reaction plate and data were analysed using the 2-ΔΔCT method. The purity of the amplified product was verified by analysing the melt curve obtained at the end of amplification. For mouse experiments, human ribosomal protein L19 (*Rpl19*) and ribosomal protein L27 (*Rpl27*), the murine hypoxanthine guanine phosphoribosyl transferase (*Hprt*) or *Hprt* combined to the Ornithine decarboxylase antizyme 1 (*Oaz1*), using a geometric mean approach [39], were used as housekeeping genes respectively for tumour derived from human cancer cells, subcutaneous, epididymal and mesenteric adipose tissue. Human *Rpl27* and *Rpl19*, and murine ribosomal protein L6 (*Rpl6*), were used respectively as housekeeping genes for human FaDu, SiHa and HCT116 cancer cells and for murine C26 and LLC. Primer sequences are listed in Table S2.

2.8. Western blot analyses on adipose tissues

Total protein was extracted from adipose tissues using RIPA buffer containing phosphatase and protease inhibitors. Adipose tissue (50 mg) was homogenized in 300 μl of RIPA buffer using a Tissue Lyser. The homogenate was mixed under end-over-end rotation (20 min 4 °C) and incubated on ice for 1 h at 4 °C. Samples were centrifuged (15 min 20 000 g 4 °C) and protein supernatant was collected by removing the lipid layer. The 2 last steps were repeated twice to reduce the amount of lipid in the sample. Protein concentration was measured using Pierce™ BCA Protein Assay Kit (ThermoFisher). Total protein extracts (30 μg) were separated by 10% SDS-PAGE and transferred to nitrocellulose membranes using a Trans-Blot Turbo Transfer System (Bio-Rad, Hercules, CA, USA). Membranes were stained with Ponceau S dye for protein detection, blocked in Tris-buffered saline-Tween 20 (TBS-T) containing 5% dry milk (Régilait, France) for 1 h at room temperature and then incubated overnight with primary antibody at 4 °C under gentle agitation. Next morning, membranes were rinsed with TBS-T and incubated with secondary antibody (dilution 1/10 000; Merck, α-rabbit, IgG Antibody, Peroxidase Conjugated #AP132P or dilution 1/4000; Dako, α-mouse IgG, HRP-

linked Antibody #P0260) in 1% milk or BSA for 1 h at room temperature. Signals were revealed using the SuperSignal West Pico, analysed with the ImageQuant TL instrument (GE Healthcare, Waukesha,WI, USA) and quantified with the imaging software Image Quant TL 8.2 (GE Healthcare). When necessary, membranes were incubated in stripping buffer for 15 min at room temperature (ThermoFisher, #21059), rinsed with TBS-T, and then re-blocked. Because at least two gels were required to analyse all samples, data were normalised by the mean protein expression of two samples deposited on each gel.

Primary antibodies (dilution 1/1000 in 5% BSA or dry milk TBS-T; Cell Signaling): HSL (BSA; α-rabbit, #4107); phospho-HSL(Ser660) (dry milk; α-rabbit, #45804); phospho-HSL(Ser563) (BSA; α-rabbit, #4139); phospho-HSL(Ser565) (BSA; α-rabbit, #4137); ATGL (dry milk; α-rabbit, #2138). β-actin primary antibody (dilution 1/5000 in 1% dry milk TBS-T; Abcam, α-Mouse, #ab6276) was used as loading control.

2.9. Dosage of NEFA and glycerol

Glycerol and NEFA in adipocyte supernatants and plasma were measured using glycerol (Sigma, MAK117 and F6428; Promega, J3150) and NEFA (Randox) assay kits according to the manufacturer's protocol. *In vivo* lipolytic activity was estimated as the concentration of circulating glycerol and NEFA, normalised to total fat mass measured by TD-NMR.

2.10. Dosage of glucose and glutamine

Glutamine and glucose concentration in conditioned media were measured using glutamine (Abcam) and glucose assay kits (GOD FS, DiaSys) according to the manufacturer's protocols.

2.11. Dosage of circulating human β-glucuronidase (GUSB)

Human GUSB was measured using a GUSB ELISA kit (Invitrogen) according to the manufacturer's protocol.

2.12. Cross-sectional prospective study with cancer patients

The cohort of patients and its characterisation was previously reported [40]. This study was conducted at the Cliniques universitaires Saint-Luc (Belgium) and approved by the University-hospital Ethic committee Saint-Luc-UCL (NCT01604642).

Patients with colorectal or lung cancer were recruited at diagnosis or relapse, before any therapeutic intervention, from January 2012 to March 2014. Written consent was obtained prior to enrolment in the study. Exclusion criteria were: non-Caucasian, patients with underlying problems leading to malnutrition, major walking handicap, ECOG performance status $\geq$4 and conditions that would preclude participation in the full protocol. The cachectic status was determined using the definition proposed by Fearon et al., as an involuntary weight loss $>$5% over the past 6 months or weight loss $>$2% and BMI $<$20 kg/m^2 or weight loss $>$2% and low muscularity [41]. Fat mass was assessed by abdomen CT scan [40].

2.13. Statistical analysis

Statistical analyses were carried out using GraphPad Prism® 8.01 (La Jolla, California, USA). Normality was checked using the Shapiro—Wilk test. Outliers were excluded using Grubbs' test ($\alpha = 0.05$). Data were analysed using a Student t-test when comparing two groups, one-way ANOVA with Dunnett's post-hoc tests, or two-way ANOVA with Sidak's post-hoc tests when appropriate. For data determined to be normal without assuming equal variance, data were analysed using a Student t-test with Welch's correction when comparing two groups or using Brown-Forsythe ANOVA and Welch ANOVA tests for more than two groups. Non-normal data were analysed using a Mann—Whitney U test or Kruskal—Wallis test with Dunn's post-tests. Concerning simple correlations between 2 variables, Pearson's and Spearman's correlations were performed for normal and non-normal data respectively. For lipolysis data of murine primary adipocytes, a mixed model analysis was performed using the R packages *car* version 3.1—2 [42], *lme4* version 1.1—35.1 [43] and *lsmeans* version 2.30—0 [44]. In this model, the conditioned medium treatment was defined as fixed effect and each isolation was considered as random effect. We considered $p \leq 0.05$ to be statistically significant.

3. RESULTS

3.1. Acid-exposed cancer cells foster lipolysis in primary subcutaneous and mesenteric adipocytes

To evaluate the prolipolytic capacities of acid-exposed cancer cells, cancer cell lines from human origin, HCT116, SiHa, FaDu, MIA PaCa-2 and PANC-1, and from murine origin, C26 and LLC, were adapted to pH6.5 (pH6.5/cancer cells) while naive cells were maintained at pH7.4 (pH7.4/cancer cells). Primary mouse adipocytes from subcutaneous (SAT) and mesenteric adipose tissues (MAT) were exposed to conditioned medium from pH6.5/and pH7.4/cancer cells (Figures 1, S1). Importantly, the conditioned media were buffered at pH7.4 before adipocyte treatment to exclude a direct pH-related effect and only evaluate the impact of factors released by acid-exposed cancer cells (Fig. S1c—f). Conditioned medium from the above acid-exposed cancer cells (except PANC-1 and C26 cells) triggered an increase in lipolysis, measured *via* glycerol release, from subcutaneous and visceral mesenteric primary adipocytes. Both types of adipocytes exhibited a similar response if not the strongest response in subcutaneous adipocytes in SiHa (at 48 h) and LLC (Table S3).

Altogether, these results highlight that acid-exposed cancer cell lines are more likely to promote lipolysis in adipocytes *via* the release of soluble factors.

3.2. Acidosis adaptation promotes mRNA expression of exogeneous fatty acid import markers

We addressed the fatty acid metabolism shift in pH6.5/FaDu, SiHa, HCT116, C26 and LLC under fatty acid-free conditions through non-targeted (only in human cancer cells) and targeted transcriptomic approaches. Principal component analysis on transcriptomics data obtained from FaDu, SiHa and HCT116 highlighted a clear separation between pH6.5/and pH7.4/cancer cells (Figure 2A—B). PC1 and PC2 accounted for the origin of the cell lines while PC3 revealed the contribution of acidosis to the variance in the dataset. Accordingly, a PERMANOVA analysis indicated that acidosis adaptation explained 9% of the variance ($p = 0.033$) while cell origin explained 54% of the variance ($p = 0.001$). Acid exposure modified the expression of 8587, 4603 and 8992 genes respectively in FaDu, SiHa and HCT116 cells with 684 genes commonly affected [padj $<$0.05; log2 fold change $>$0.3] (Figure 2C, full list in Table S4). Among these 684 genes, 404 genes shared similar changes of direction, with 212 genes commonly overexpressed and 192 genes commonly downregulated. Mapping of main lipid metabolism pathways identified significant alterations in pH6.5/cancer cells (Figures 2D and S2). An upregulation of fatty acid uptake was observed with consistent *Cd36* (*cluster of differentiation 36*) increase in all pH6.5/cancer cells, but also cell type-dependent changes in other actors of fatty acid uptake (Figures 2D, S2 and 3). For instance, *fatty acid binding protein 4* (*Fabp4*) expression was enhanced in C26 and LLC cells, and *transforming growth factor β2*, *tgfβ2*, which has been previously identified as a driver of the uptake

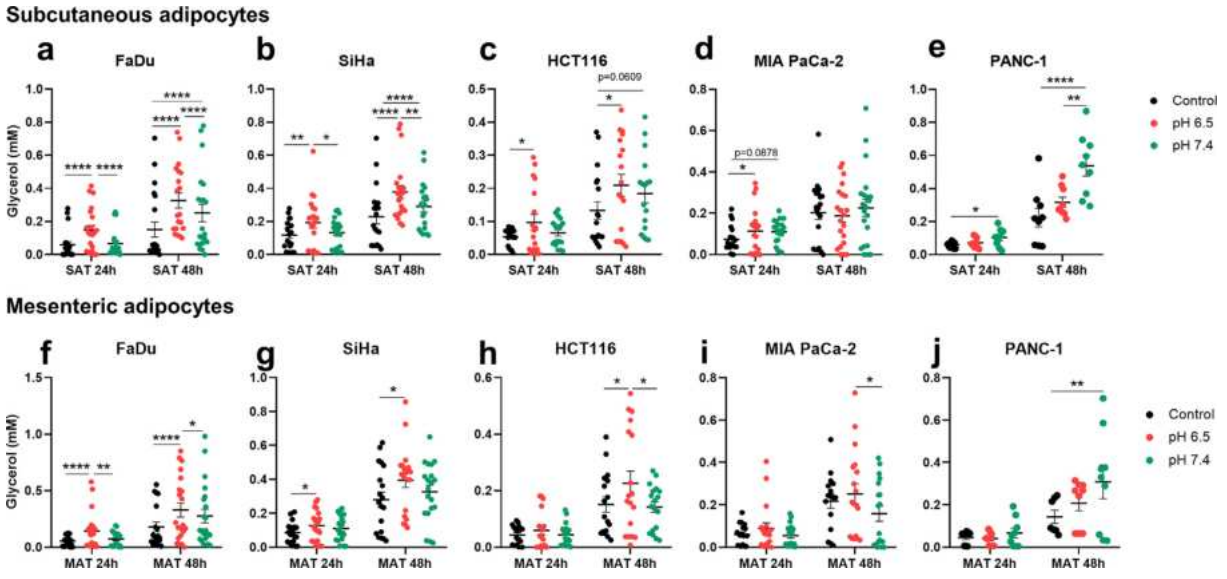

Figure 1: Conditioned medium from human acid-exposed cancer cells induces subcutaneous and mesenteric adipocyte lipolysis. Treatment of subcutaneous (SAT, top panel, a-e) and mesenteric (MAT, bottom panel, f-j) *ex-vivo* adipocytes, from male C57BL/6, with conditioned medium from human pH7.4/(in green) and pH6.5/cancer cells (in pink), FaDu (a,f), SiHa (b,g), HCT116 (c,h), MIA PaCa (d,i), and PANC-1(e,j), for 24 h or 48 h. In the control condition, adipocytes were treated with control medium collected in parallel to the conditioned medium. The glycerol level reflects lipolysis. The glycerol level was normalised to the number of cancer cells used for preparation of the conditioned medium. FaDu, human hypopharyngeal cancer cells; SiHa, human cervix cancer cells; HCT116, human colon cancer cells; MIA PaCa-2 and PANC-1, human pancreatic cancer cells. Data are presented as the mean ± SEM. n = 6–7 (except for PANC-1, n = 3). Each point represents a replicate. *p < 0.05, **p < 0.01, ****p < 0.0001.

and storage of fatty acids in acid-exposed cancer cells [5], was increased in pH6.5/FaDu and LLC. Transcriptomic analysis also revealed that the fate of fatty acids was not restricted to storage as triglycerides in lipid droplets (as in HCT116, SiHa, C26, LLC) but also encompassed oxidation in mitochondria and/or peroxisomes (HCT116, FaDu). Consistent with an increase in fatty acid import, human pH6.5/FaDu, SiHa and HCT116 exhibited a decreased fatty acid synthesis with a downregulation of *fatty acid synthase* (*Fasn*), the final enzyme of *de novo* lipogenesis (Figures 2 and 3D and S2). In line with previous RNAseq studies conducted in pH6.5/cancer cells cultured in the presence of fatty acids [4], our transcriptomic analyses in cells deprived of exogenous fatty acids underscore the preference of acidosis-adapted cancer cells for exogeneous fatty acids rather than endogenous fatty acid synthesis to fulfil their lipid requirements.

As a consequence of greater dependence on fatty acids under acidosis, pH6.5/cancer cells consumed generally less glutamine and glucose than pH7.4/cancer cells (Fig. S1g–h). As glucose and glutamine can both modulate lipolysis [45,46], we next aimed to determine to which extent this reduced nutrient consumption may explain the enhanced prolipolytic ability of acid-adapted cancer cells. Primary mouse adipocytes were exposed to medium containing the same levels of glucose and glutamine than the ones present in the conditioned medium of pH6.5/and pH7.4/HCT116 for 48 h. No difference in the lipolytic response were observed between both conditions (Fig. S1i). We therefore concluded that the altered depletion of nutrients is not driving the enhanced prolipolytic ability of acid-exposed HCT116.

3.3. Tumoral acidosis is associated to an enhanced lipolysis *in vivo* leading to a loss of adipose tissue

Human colon HCT116 and pharynx FaDu cancer cells were previously reported to generate tumours exhibiting a pH gradient in mice [47–53]. HCT116 tumour-bearing mice developed cachexia, in parallel to tumour growth, with a decrease in fat mass starting 14 days post-HCT116 injection, earlier than the reduction of body weight and food intake starting from 15 days post-HCT116 injection (Figure 4A–E). In adipose tissues localized from the closest to the farthest from the tumour (developing in the right anterior flank), we observed significant reductions of 54% in right anterior, 50% in left anterior, 46% in posterior SAT, and 32% and 48% in visceral EAT and MAT, respectively (Figure 4F–J). Both close and distant adipose tissues were depleted with higher fat loss in the closest adipose tissues. Interestingly, this fat mass loss precedes lean mass depletion, which occurred 16 days post-HCT116 cell injection with a 13% and 15% reduction in the gastrocnemius and tibialis muscles, respectively (Figure 4K–N). This adipose tissue depletion was accompanied by a 2.5–3 fold increase in *in vivo* lipolytic activity, measured as the concentration of plasma NEFA and glycerol normalised to the amount of total fat mass [20] (Figure 5A–B). We next aimed to evaluate whether this increased lipolytic activity resulted from an increased expression or activity of lipolytic enzymes. Markers of lipolysis inhibition were decreased in adipose tissues closer from the tumour, with a trend and a significant decrease of phospho-HSL565, normalised to HSL, in right and left anterior SAT. At distance from the tumour, the MAT presented an increase of markers of lipolysis activation, with an upward trend for ATGL and a significant increase of phospho-HSL660 normalised to β-actin (Figures 5C–H and S3). The increase of ATGL protein in MAT was supported by a higher *Atgl* mRNA expression. Nonetheless, ATGL and HSL protein expressions were not altered in posterior subcutaneous and visceral adipose tissues. *Lipa* (gene encoding the LAL protein), a lysosomal lipolytic enzyme, was increased in MAT and EAT. We explored mediators of lipolysis such as fat-specific protein 27 (Fsp27) and G0/G1 switch 2 (G0S2), two ATGL inhibitors, and the comparative gene identification-58 protein (CGI-58) which recruit and activate ATGL [18] (Fig. S4). Interestingly, *Cgi-58* mRNA expression increased consistently in posterior SAT, MAT and EAT and would be a key mediator of their lipolysis by activating ATGL. In conclusion, we found tissue-specific changes that associated with tissue location from the tumour, with a lower inhibition of lipolysis in adipose tissues close to

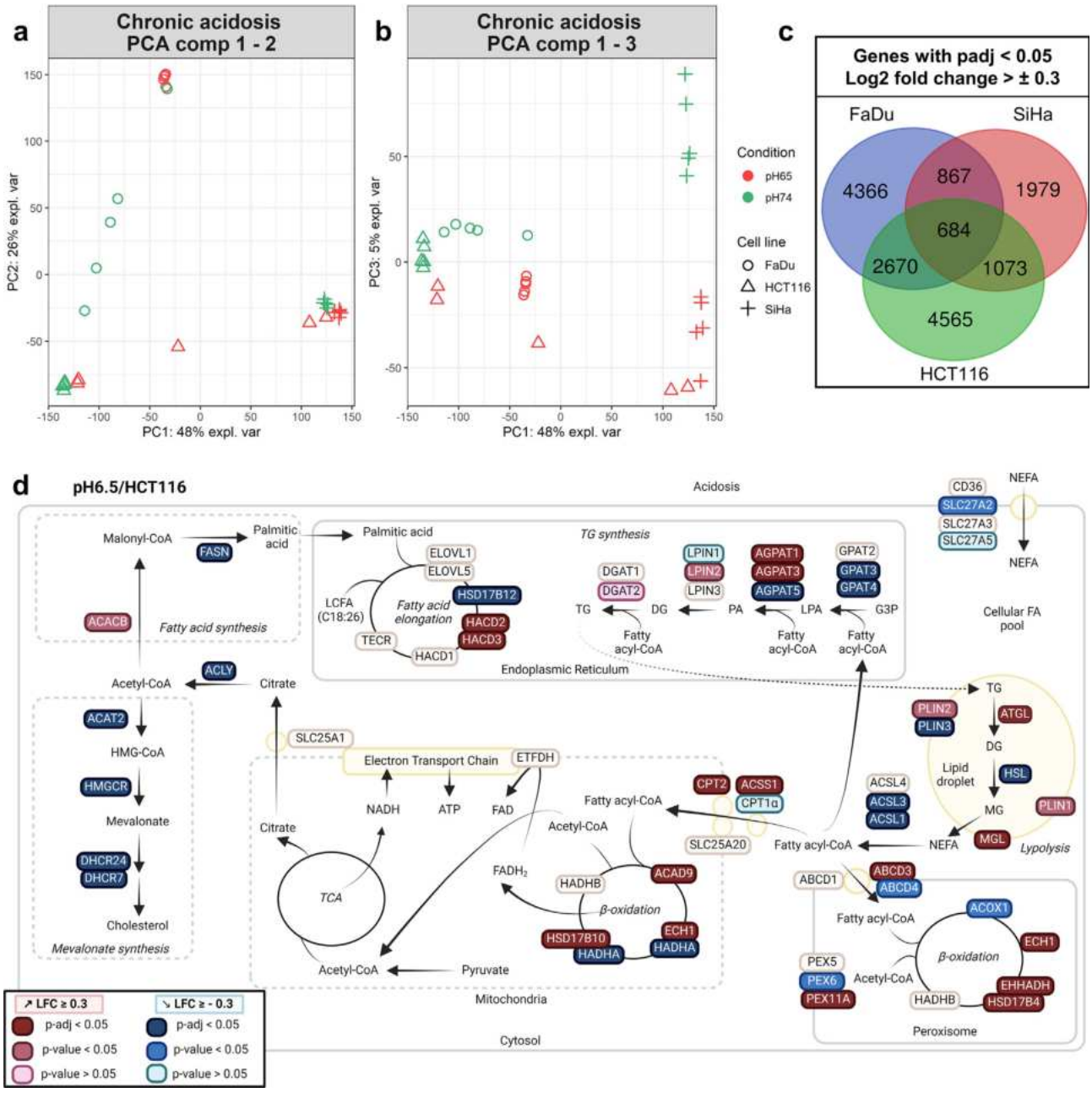

Figure 2: Acidosis adaptation impacts the cancer cell transcriptome, including their fatty acid metabolism pathways. (a, b) Principal Component Analyses (PCA) performed on gene expression in human pH6.5/(pink) and pH7.4/FaDu (circle), SiHa (cross) and HCT116 (triangle) cancer cells (green), depicting PC1 and 2 (a) and PC1 and 3 (b). (c) A Venn diagram was generated from genes differentially expressed between human pH6.5/and pH7.4/FaDu, SiHa and HCT116 cancer cell lines (d) Overview of the expression level of genes involved in fatty acid metabolism in pH6.5/HCT116 compared with pH7.4/HCT116 (adapted from Rolver et al., 2023 [4]). Colour indicates p-adj, p-value and average log2 fold change (LFC) across 5 replicates per condition. ABCD1/3/4, ATP binding cassette subfamily; ACACB, acetyl-CoA carboxylase beta; ACAD9, acyl-Coa dehydrogenase 9; ACAT2, acetyl-CoA acetyltransferase 2; ACLY, ATP citrate lyase; ACOX1, acyl-CoA oxidase 1; ACSL1/3/4, acetyl-CoA synthethase long chain 1/3/4; AGPAT1/3/5, 1-acylglycerol-3-phosphate O-acyltransferase 1/3/5; ATGL, adipose triglyceride lipase; CD36, cluster of differentiation 36 or fatty acid translocase; CPT1α/2, carnitine palmitoyltransferase 1alpha/2; DG, diglyceride; DGAT1/2, diacylglycerol O-acyltransferase 1/2; DHCR7/24,7/24-dehydrocholesterol reductase; ECH1, enoyl-CoA hydratase 1; EHHADH, enoyl-CoA hydratase and 3-hydroxyacyl CoA dehydrogenase; ELOVL1/5, ELOVL fatty acid elongase 1/5; ETFDH, electron transfer flavoprotein dehydrogenase; FA, fatty acid; FaDu, human hypopharyngeal cancer cells; FASN, fatty acid synthase; G3P, glycerol-3-phosphate; GPAT2/3/4, glycerol-3-phosphate acyltransferase 2/3/4; HACD1/2/3, 3-hydroxyacyl-CoA dehydrogenase 1/2/3; HADHA/B, hydroxyacyl-CoA dehydrogenase trifunctional multienzyme complex subunit alpha/beta; HCT116, human colon cancer cells; HMGCR: 3-hydroxy-3-methylglutaryl-CoA reductase; HSD17B4/10/12, hydroxysteroid 17-beta dehydrogenase 4/10/12; HSL, hormone-sensitive lipase; LCFA, long chain fatty acid; LPA, lysophosphatidic acid; LPIN1/2/3, Lipin 1/2/3; NEFA, non-esterified fatty acids; MGL, monoglyceride lipase; PA, palmitic acid; PEX5/6/11A, peroxisomal biogenesis factor 5/6/11 alpha; PLIN2/3, Perilipin 2/3; SLC25A1/20, solute carrier family 25 member 1/20; SiHa, human cervix cancer cells; SLC27A1/3/5, solute carrier family 27 member 1/3/5; TECR, trans-2,3-enoyl-CoA reductase; TG, triglyceride. Created with BioRender.com.

the tumour and a common increase of *Cgi-58* in adipose tissues distant from the tumour. In FaDu tumour-bearing mice, adipose tissues were collected when the tumour reached 2000 mm^3 or on day 44 post-injection for the last mice (Fig. S5). FaDu injection promoted EAT loss without affecting body weight and food intake, and independently of muscle atrophy. Regarding *in vivo* lipolysis activity, NEFA levels were

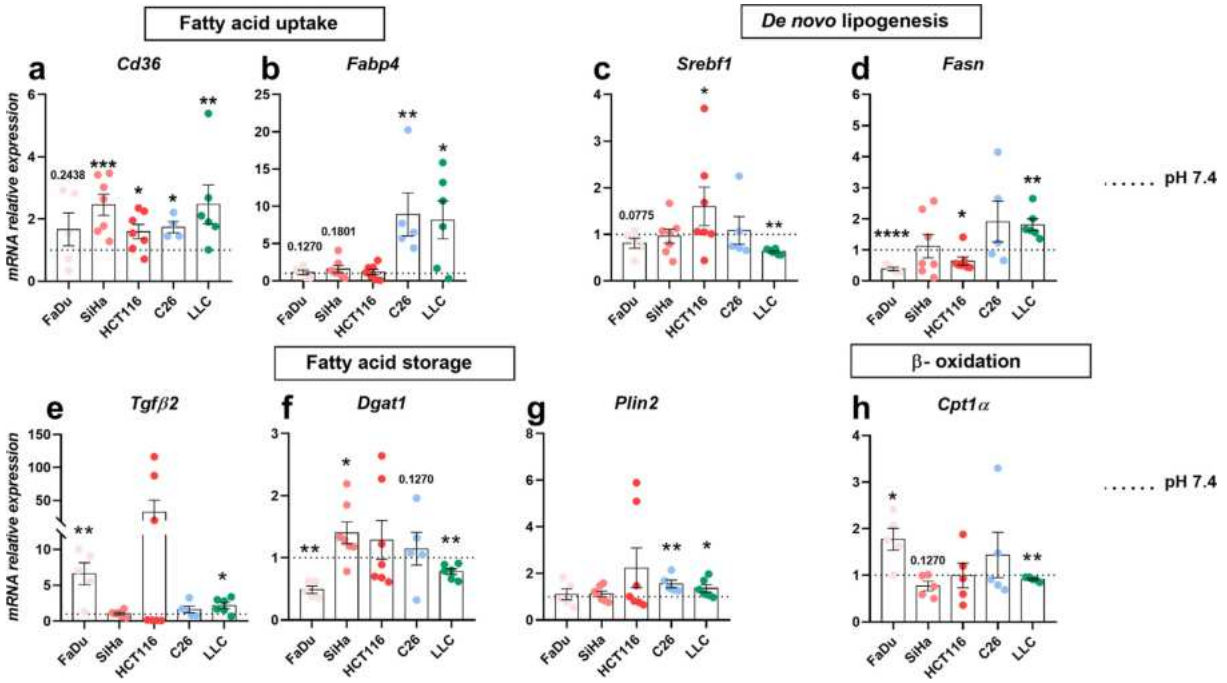

Figure 3: Acidosis adaptation promotes exogenous fatty acid import rather than endogenous fatty acid synthesis. mRNA relative expression of fatty acid uptake genes, *Cd36* (a) and *Fabp4* (b), *de novo* lipogenesis genes, *Srebf1* (c) and *Fasn* (d), fatty acid storage genes, *Tgfβ2* (e), *Dgat1* (f) and *Plin2* (g), and β-oxidation gene, *Cpt1α* (h), in human pH6.5/cancer cells, FaDu, SiHa, HCT116, and in murine pH6.5/C26 and LLC. Gene expression in pH6.5/cancer cells was expressed relative to the mean gene expression in pH7.4/cancer cells (pH7.4 = 1; dotted line). *Cd36*, cluster of differentiation 36 or fatty acid translocase; *Fabp4*, fatty acid binding protein 4; *Srebf1*, sterol regulatory element binding transcription factor 1; *Fasn*, fatty acid synthase; *Tgfβ2*, transforming growth factor beta 2; *Dgat1*, diacylglycerol O-acyltransferase 1; *Plin2*, perilipin 2; *Cpt1α*, carnitine palmitoyltransferase 1A. FaDu, human hypopharyngeal cancer cells; SiHa, human cervix cancer cells; HCT116, human colon cancer cells; C26, murine colon cancer cells; LLC, Lewis lung carcinoma cells. Data are presented as the mean ± SEM. n = 4–7. Each point corresponds to one n. *p < 0.05, **p < 0.01, ***p < 0.001, ****p < 0.0001.

increased by 1.60 in FaDu tumour-bearing mice, while glycerol levels were unaffected. Altogether, these results indicate that HCT116 are more prone to induce adipose tissue breakdown than FaDu tumours.

To explore the association between tumoral acidosis and adipose tissue depletion, we first reasoned that larger was a tumour, more pronounced was the ambient tumour acidosis. Using the tumour weight however failed to identify a correlation with the extent of adipose tissue loss (Figure 6C), except with right and left anterior SAT (ie, the closest adipose tissues from tumours). We therefore used pHLIP, a pH-low insertion peptide to more directly evaluate, upon mouse injection, the extent of acidosis in HCT116 tumours (Figure 6A–C) [5,26]. We found that the percentage of pHLIP-positive cells did not correlate with tumour weight ($r = 0.2780$, $p = 0.38$). By computing a pHLIP score combining the percentage of cells positive for pHLIP and the tumour weight, we found a more pronounced trend towards a negative correlation in distant adipose tissues with however a statistical significance only for posterior SAT.

In FaDu tumour-bearing mice, instead of pHLIP we used *Mct4* (*monocarboxylate Transporter 4*) gene expression as a marker of tumour hypoxia and thus a reasonable marker of acidosis considering its dual lactate/H^+ symporter function [2]. *Mct4* negatively correlated very closely with left anterior and posterior SAT and EAT; a similar trend was observed for right anterior SAT and MAT (Fig. S5i).

Altogether, these data strongly suggest a link between tumoral acidosis and adipose tissue loss in mice.

3.4. Neutralisation of tumoral acidosis with sodium bicarbonate prevents adipose tissue depletion *in vivo*

To explore more formally the contribution of tumoral acidosis to adipose tissue depletion, HCT116 tumour-bearing mice were treated for 14 days with 200 mM sodium bicarbonate ($NaHCO_3$) in drinking water to dampen tumoral acidosis (Figures 6F–K and S6). Necropsy was carried out at the onset of fat mass loss in HCT116 tumour-bearing mice without $NaHCO_3$ treatment, before any decrease in food intake to avoid the interference of anorexia. This necropsy at an earlier stage of cachexia led to a more modest reduction in adipose tissue weight (Figures 4D, S6e). A delay of ~4 days in tumour growth was recorded compared to the previous experiment (Fig. S6a), which explains the lower fat mass loss despite the necropsy being carried over 18 days post-injection versus 16 days for the previous experiment. Tumour weight at necropsy and systemic pH were not affected by $NaHCO_3$ treatment (Figures 6E–F and S6a).

To address the $NaHCO_3$ effect on neutralisation of tumour acidosis, we explored both pH homeostasis mediators and fatty acid metabolism in the HCT116 tumour. The mRNA expression of the lysosomal associated membrane protein 2, LAMP2, reported to increase under acidosis [54], was decreased under bicarbonate treatment (Fig. S6l–n). This reduction was accompanied by an increase of *Mct4* expression probably to facilitate the export of H^+ and increase the pH in the HCT116 tumour. The increase in mRNA expression of CA2, the carbonic anhydrase 2, would be a straight response to $NaHCO_3$ treatment. Indeed, CA2 can increase the intracellular pH by catalysing the reaction transforming HCO_3^- and one proton H^+ into CO_2 and H_2O [1]. Moreover, the bicarbonate administration would reduce the fatty acid dependency associated to acidosis in the HCT116 tumour with a decrease of *Fabp4* and *Fasn* (Fig. S6o–q). Altogether, these data suggest that tumour acidosis was neutralised by $NaHCO_3$.

The administration of bicarbonate protected against total fat mass loss by preventing adipose tissue depletion induced by HCT116 injection in anterior left and posterior SAT, EAT and MAT (Figures 6G–K and S6g–k).

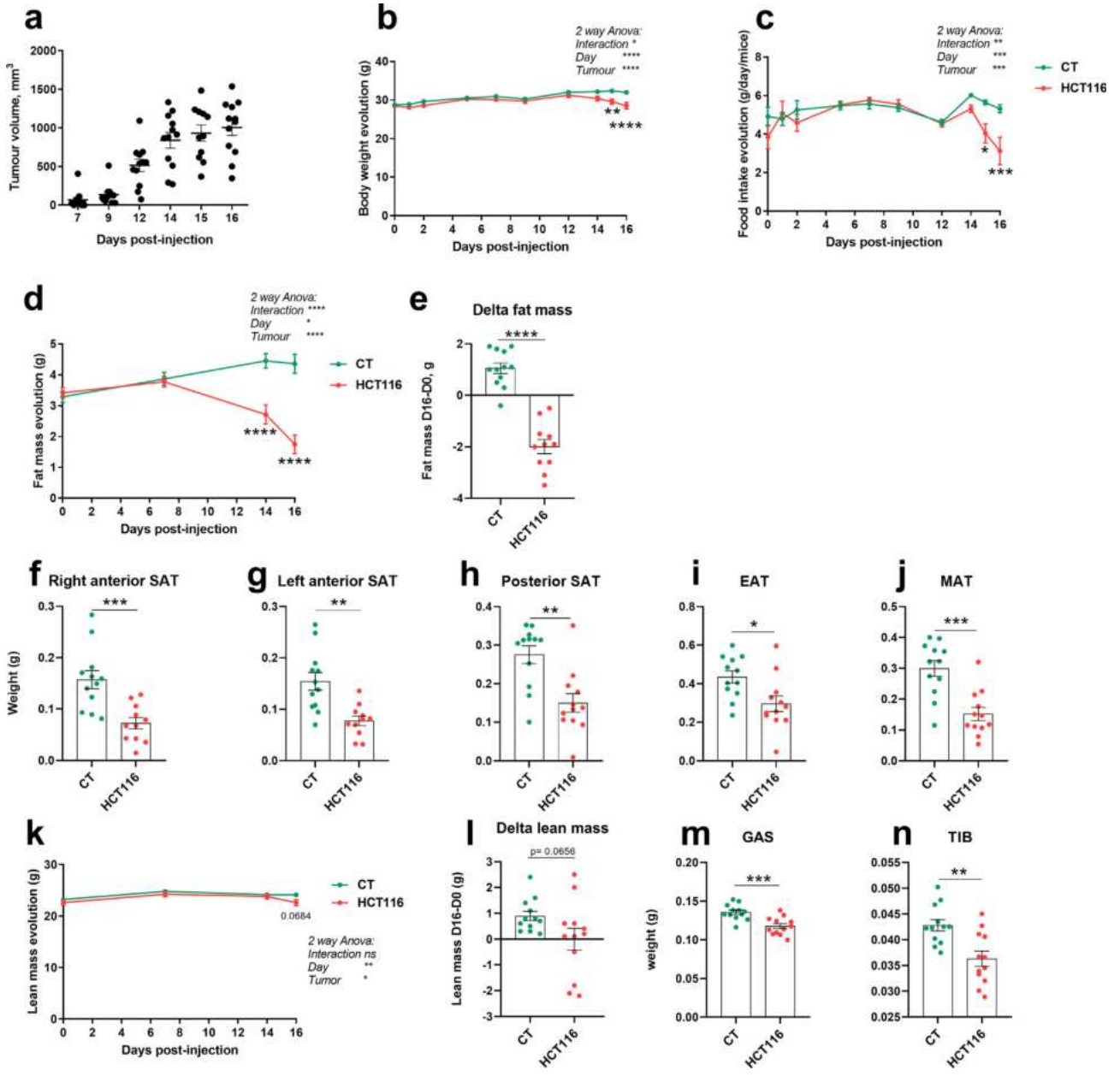

Figure 4: HCT116 cells promote adipose tissue depletion before lean mass loss *in vivo*. Evolution of tumour volume (a), body weight (b), food intake (c) and fat mass (d) in male sham-injected mice (CT) and mice injected with human colon HCT116 cancer cells (HCT116), for 16 days post-injection. (e) Delta fat mass between day 16 post-injection (necropsy) and day 0 in CT and HCT116 tumour-bearing mice. Right anterior (f), left anterior (g) and posterior (h) subcutaneous adipose tissue (SAT), visceral epididymal (i, EAT) and mesenteric (j, MAT) adipose tissue weights in CT and HCT116 tumour-bearing mice at necropsy. (k) Evolution of lean mass for 16 days post-injection. (l) Delta lean mass between the day of necropsy and day 0 in CT and HCT116 tumour-bearing mice. Gastrocnemius (m) and tibialis (n) weights at necropsy. Data are presented as the mean ± SEM. Each point corresponds to one mouse (n = 11–12) or mean food intake per cage (n = 6). *p < 0.05, **p < 0.01, ***p < 0.001, ****p < 0.0001.

Besides, $NaHCO_3$ administration prevents the *Atgl* mRNA expression increase in MAT (Figure 6L). This was not associated to a decrease of tumoral known prolipolytic factors *Il6, Tnfα, Zag* or *Pthlh* mRNA expression (Fig. S6r–u). The above findings support a role for tumoral acidosis in adipose tissue depletion.

3.5. Tumoral acidosis promotes the expression of GUSB, a newly identified prolipolytic factor *in vitro*

To identify prolipolytic mediators released by acid-exposed cancer cells that may reach out to adipose tissues, we first examined a set of known prolipolytic mediators, namely IL6, TNFα, ADM, ZAG, PTHLH and Proliferin-1 [11,19,23]. Proliferin-1 is a protein member of the growth hormone/prolactin gene family, encoded by *Prl2c* (prolactin family 2, subfamily c) gene only expressed in mice, but humans presents proliferin-1-like molecules that could have similar effect [23]. The patterns and number of upregulated pro-lipolytic mediators vary with the nature of acid-exposed cancer cells. For instance, pH6.5/HCT116 cells exhibited high levels of several factors (ie, *Il6*, *Tnfα*, *Zag* and *Pthlh*) while pH6.5/SiHa cells displayed no change (Figure 7A–F). In a second step, to pinpoint potentially new prolipolytic mediators shared between pH6.5/cancer cells, we took advantage of our transcriptomics analysis to identify commonly predicted secreted proteins

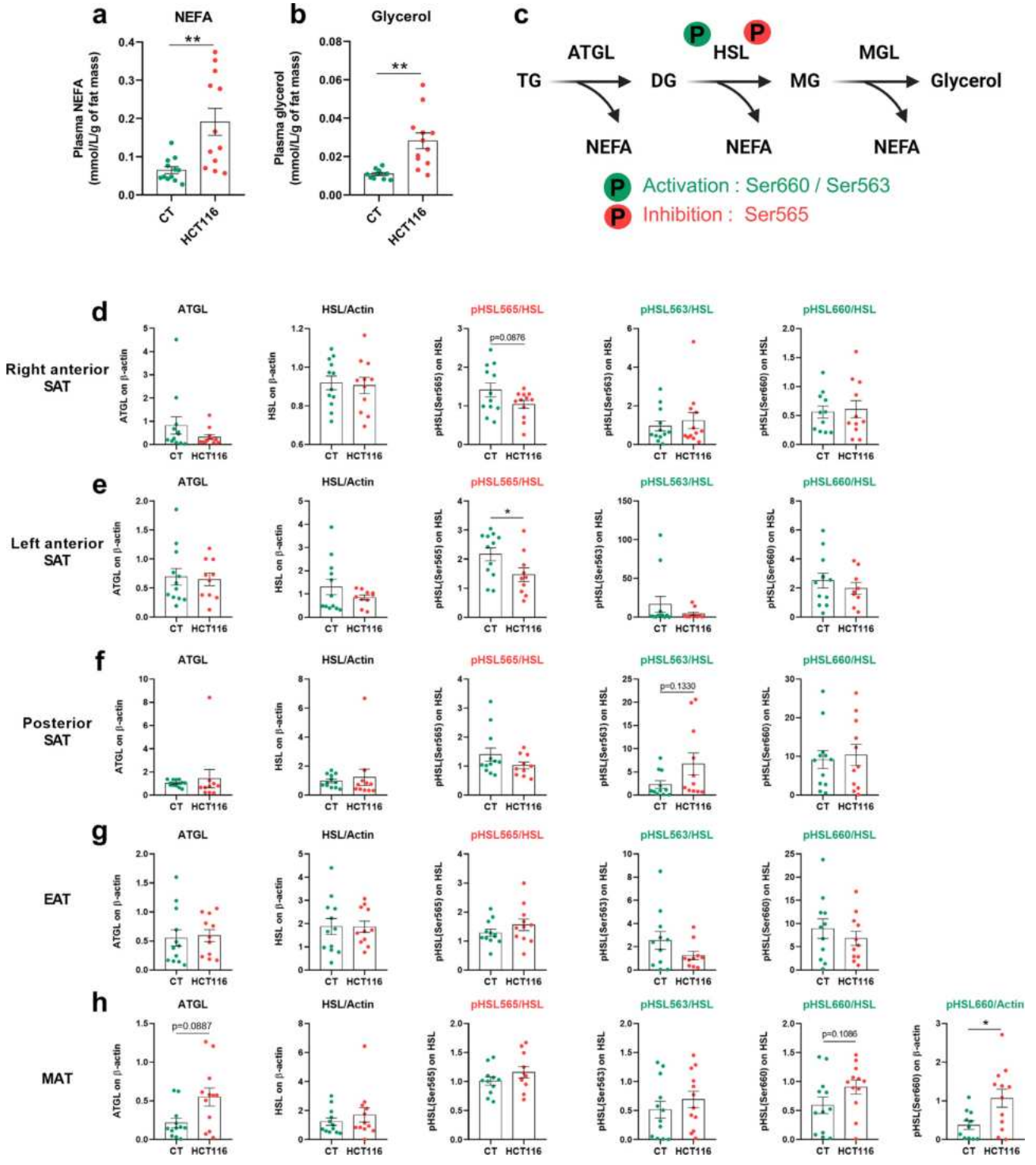

Figure 5: HCT116 tumour induces adipose tissue lipolysis *in vivo*. Plasma non-esterified fatty acids (NEFA, a) and glycerol (b) concentrations on amount of total fat mass measured by NMR on day 16 of necropsy in male sham- (CT) and HCT116-injected mice (HCT116). (c) Representative figure of the 3 steps of adipose lipolysis; ATGL and HSL are the limiting enzymes of adipose lipolysis. ATGL catalyzes the transformation of triglycerides (TG) into diacylglycerides (DG), HSL transforms the DG into monoacylglycerides (MG). HSL is regulated by phosphorylation, either by activating (on Ser660 and Ser563, in green) or inhibiting (on Ser565, in pink) adipose lipolysis. MGL converts DG into glycerol. Each step of adipose lipolysis releases one NEFA. (d–h) Protein expression of lipolysis enzymes, ATGL, non-phosphorylated HSL, phosphorylated HSL; inhibitor (pHSL565, in pink) or activator of lipolysis (pHSL563 and pHSL660, in green), in right anterior (d), left anterior (e) and posterior (f) subcutaneous SAT, visceral epididymal (EAT, g) and mesenteric (MAT, h) adipose tissues on the day of necropsy in CT and HCT116 tumour-bearing mice. ATGL and HSL were normalised to β-actin and phosphorylated HSL (pHSL) on HSL and to β-actin for pHSL560. NEFA, non-esterified fatty acids; NMR, nuclear magnetic resonance; HCT116, human colon cancer cells; ATGL, adipose triglyceride lipase; HSL, Hormone-sensitive lipase; pHSL, phosphorylated HSL; MGL, monoglyceride lipase; TG, triglyceride; DG, diacylgyceride; MG, monoglyceride; Ser, serine; SAT, subcutaneous adipose tissue; EAT, epididymal adipose tissue; MAT, mesenteric adipose tissue. Data are presented as the mean ± SEM. n = 10–12. Each point corresponds to one mouse. *$p < 0.05$, **$p < 0.01$.

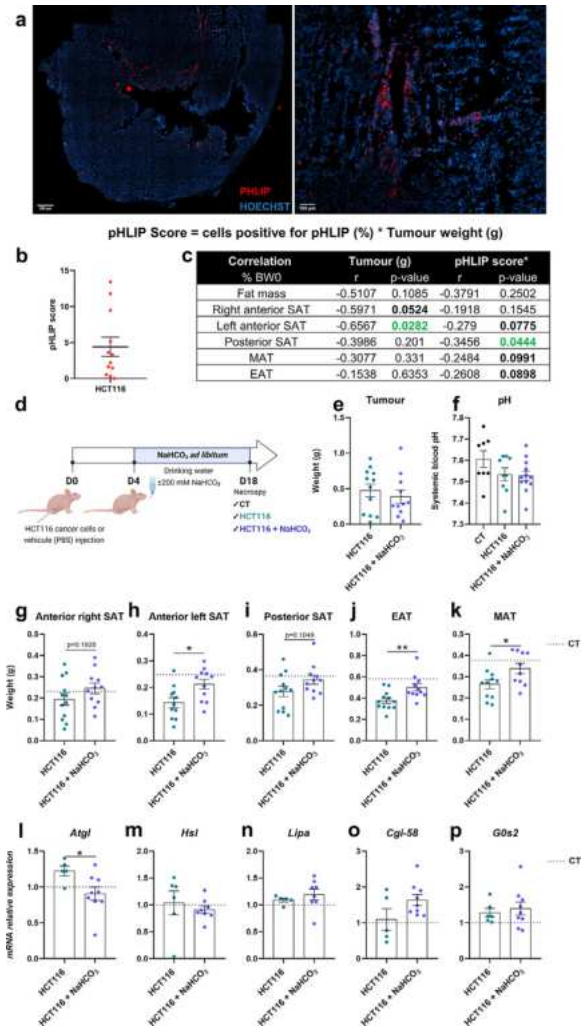

Figure 6: Tumoral acidosis associates with adipose tissue weights in HCT116 tumour-bearing mice and neutralisation of acidosis with bicarbonate prevents adipose tissue weight loss. (a) Representative full (left panel) and enlarged (right panel) longitudinal tumour sections from male HCT116 tumour-bearing mice at day 16 post-injection (necropsy) with fluorescent staining for pHLIP (in red), a pH-low insertion peptide with properties to high targeting the tumoral acidosis, and for Hoechst (in blue), a nucleus dye. (b) pHLIP score at day of necropsy in HCT116 tumour-bearing mice. (c) Correlations of fat mass, right anterior, left anterior, posterior subcutaneous (SAT), visceral epididymal (EAT) and mesenteric (MAT) adipose tissues (in % BW0) with tumour (in g) and pHLIP score in HCT116 tumour-bearing mice. In green bold $p < 0.05$, in bold $p < 0.1$. (d) Male sham- (CT) and HCT116-injected mice were treated for 14 days without (HCT116) or with 200 mM sodium bicarbonate (HCT116 + $NaHCO_3$) in drinking water starting from 4 days post HCT116-injection. Necropsy was performed on day 18 post-HCT116 injection. Tumour weight (e) and Systemic blood pH (f) on day 18 of necropsy. Right anterior (g), left anterior (h), posterior (i) SAT, visceral EAT (j) and MAT (k) adipose tissue weights at necropsy. (g–k) The mean adipose tissue weight in control mice was represented by a dotted line. (l–p) MAT adipose tissue mRNA relative expression of lipolysis genes, *Atgl* (l), *Hsl* (m), *Lipa* (n), *Cgi-58* (o), *G0s2* (p) in male HCT116 tumour-bearing mice without (HCT116) or without $NaHCO_3$ treatment (HCT116 + $NaHCO_3$). (l–p) Gene expression in HCT116 tumour-bearing mice was expressed relative to the mean gene expression in the sham-injected control mice (CT = 1, dotted line). HCT116, human colon cancer cells; BW0, body weight on day 0 of HCT116 injection; *Atgl*, adipose triglyceride lipase; *Hsl*, hormone sensitive lipase; *Mgl*, monoglyceride lipase; *Lipa*, Lipase A, Lysosomal Acid Type; *Cgi-58*, comparative gene identification-58 protein; *G0s2*, G0/G1 Switch 2. Data are presented as the mean ± SEM. n = 5–12. Each point corresponds to one mouse. *$p < 0.05$, **$p < 0.01$, ***$p < 0.001$. Created with BioRender.com.

that are increased upon acidosis adaptation. 86 predicted secreted proteins were identified from the 684 altered genes shared between FaDu, SiHa and HCT116 (Figure 7G–I). Among them, only 24 were consistently overexpressed in the 3 cell lines (Figure 7J–M). Principal component analysis on predicted secreted proteins confirmed a clear separation between pH6.5/cancer cells and pH7.4/cancer cells, with cell origin and acidosis explaining 59% ($p = 0.001$) and 9% of the variance ($p = 0.034$) (Figure 7H–I). The expression of the 24 overexpressed predicted secreted proteins was correlated with glycerol release (Fig. S7). Based on these correlations and a literature search, 13 secreted proteins were selected for further exploration. Specifically, proteins not positively correlated with glycerol release, previously associated with decreased lipolysis, or documented to display lower levels in cancer, were discarded. Among the 13 selected proteins, we focused on 7 proteins present in the plasma: β-glucuronidase (GUSB), hexose-6-phosphate dehydrogenase (H6PD), laminin subunit α1 (LAMA1), Complements C4A and C4B, dipeptidyl peptidase 7 (DPP7) and tumour necrosis factor receptor superfamily member 1B (TNFRSF1B).

3T3-L1 adipocytes were incubated in presence of these proteins for 6 h and 24 h. Human recombinant proteins C4A, C4B, TNFRSF1B, DPP7 and LAMA1 did not induce lipolysis (Fig. S8a–j). Human recombinant H6PD was produced in a buffer that induced alone a strong lipolytic response, making the results of the incubation of 3T3-L1 adipocytes in presence of H6PD uninterpretable. As the level of H6PD was not increased in the plasma of HCT116 tumour-bearing mice or in the conditioned media, we discarded H6PD as a prolipolytic mediator involved in our setting (Fig. S8k–l). Interestingly, GUSB demonstrated prolipolytic effects on 3T3-L1 adipocytes after 6 h (300 ng/ml) and 24 h (0.3, 30 and 300 ng/ml), an effect that we confirmed in human primary subcutaneous and mesenteric adipocytes exposed to 150 ng/ml GUSB (Figure 8A–B). In accordance with our hypothesis, plasma GUSB levels were increased in HCT116 tumour-bearing mice and negatively correlated with the weight of posterior SAT and MAT (Figure 8C–D). The levels of GUSB increased in the pH6.5/HCT116 conditioned medium but not in the pH6.5/FaDu and pH6.5/SiHa conditioned media (Figure 8E). Consistently, no change in plasma human GUSB was observed in FaDu tumour-bearing mice (Figure 8F). In contrast, neither *Gusb* mRNA expression in the tumour nor circulating GUSB protein levels were modulated in bicarbonate-treated HCT116 tumour-bearing mice (Figure 8G–H). Of note, circulating levels of GUSB were not increased in HCT116 tumour-bearing mice at this early stage of fat mass loss.

Overall, we demonstrated that acid-exposed cancer cells exhibit an increase in the expression of a panel of known prolipolytic factors, although unshared between cancer cell lines. Furthermore, we identified GUSB as a promising new key player in the promotion of adipocyte lipolysis.

3.6. *In vivo* lipolysis was increased in cachectic patients with colon and lung cancer but negatively associated with plasma human GUSB

Finally, to further explore the role of GUSB in cachectic patients, we measured plasma GUSB in cachectic (C) and non-cachectic (NC) patients with colorectal or lung cancer. Cachectic patients displayed increased lipolytic activity than non-cachectic patients, as evidenced by higher levels of plasma glycerol levels normalised to fat mass (Fig. S9a–c). Plasma GUSB levels were unchanged between cachectic and non-cachectic patients, independently of cancer type (Fig. S9d–f). Strikingly, plasma GUSB levels correlated positively with fat mass and body mass index, and negatively with body weight loss and lipolytic activity (Fig. S9g–j). We therefore looked at plasma GUSB levels

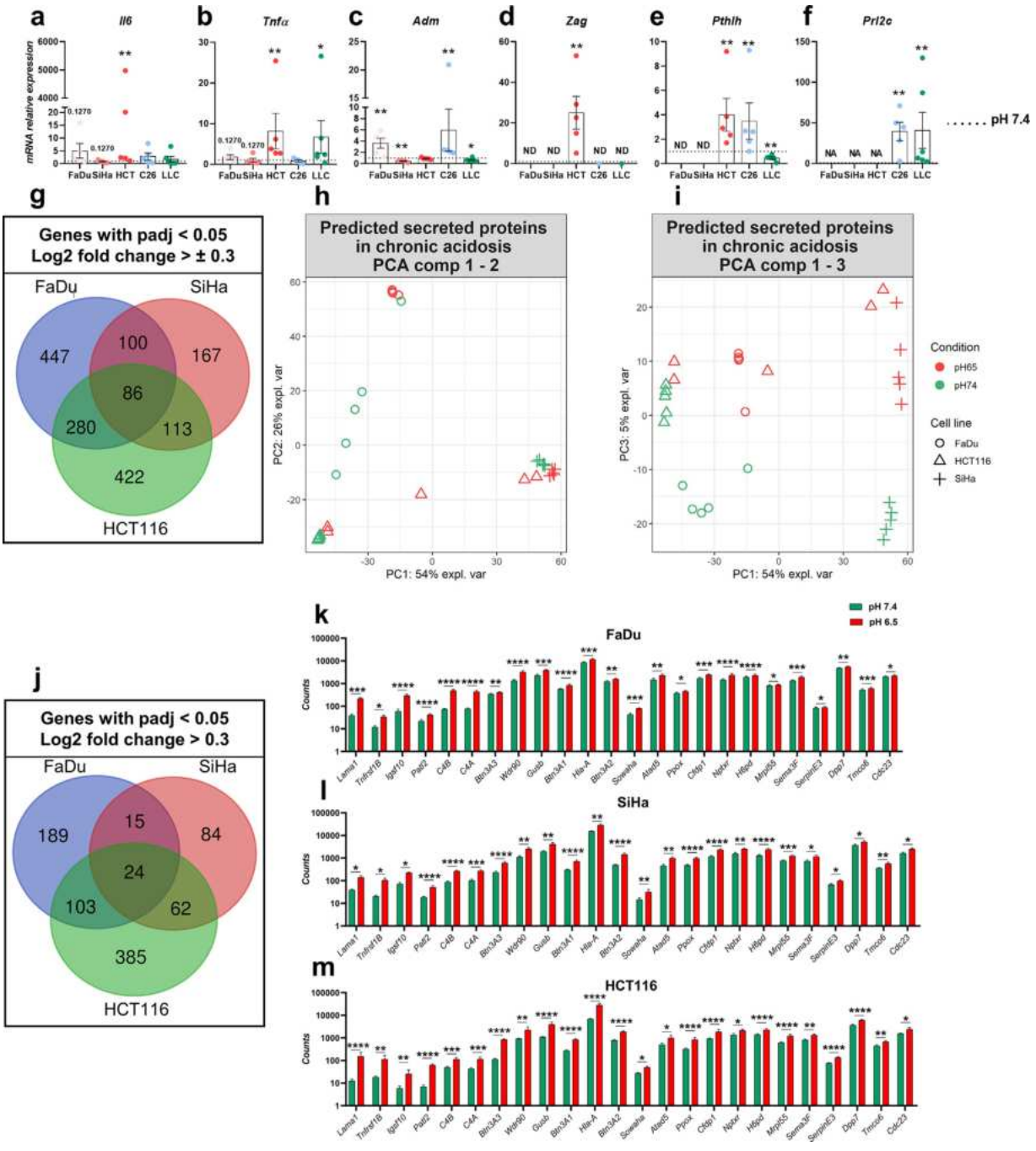

Figure 7: Expression of known prolipolytic factors and predicted secreted proteins in three human cancer cell lines exposed to acidosis. (a-f) mRNA relative expression of *Il6* (a), *Tnfα* (b), *Adm* (c), *Zag* (d), *Pthlh* (e) and *Prl2c* (f) in the human pH6.5/cancer cell lines, FaDu, SiHa and HCT116, and in murine pH6.5/C26 and LLC. Gene expression in pH6.5/cancer cells was expressed relative to the mean gene expression in pH7.4/cancer cells (pH7.4 = 1; dotted line). Data are presented as the mean ± SEM. n = 4–7. Each point corresponds to one n. (g, j) Venn diagrams were constructed from predicted secreted proteins differentially expressed between pH6.5/and pH7.4/FaDu, SiHa and HCT116 cancer cell lines. (h,i) Principal Component Analyses (PCA) was performed on predicted secreted proteins from human pH6.5/(pink) and pH7.4/FaDu (circle), SiHa (cross) and HCT116 (triangle) cancer cells (green) depicting PC1 and 2 (h) and PC1 and 3 (i). (k,l,m) Gene expression (in counts) of 24 predicted secreted proteins upregulated upon acidosis and shared between FaDu (k), SiHa (l) and HCT116 (m) cancer cells, ranked by the mean log2 fold change of 3 cancer cell lines. Data are presented as the mean ± SEM. (g–m). n = 5. *Il6*, interleukin 6; *Tnfα*, tumour necrosis factor alpha; *Adm*, adrenomedullin; *Zag*, zinc-alpha-2-glycoprotein; *Pthlh*, parathyroid hormone like hormone; *Prl2c*, prolactin family 2 subfamily c member 2. *Lama1*, laminin subunit alpha 1; *Tnfrsf1B*, tnf receptor superfamily member 1B; *Igsf10*, immunoglobulin superfamily member 10; *Patl2*, Pat1 homolog 2; *C4B*, complement c4b; *C4A*, complement c4a; *Btn3A3*, butyrophilin subfamily 3 member a3; *Wdr90*, wd repeat domain 90; *Gusb*, glucuronidase beta; *Btn3A1*, butyrophilin subfamily 3 member A1; *Hla-A*, major histocompatibility complex, class I, A; *Btn3A2*, butyrophilin subfamily 3 member A2; *Sowaha*, sosondowah ankyrin repeat domain family member A; *Atad5*, ATPase Family AAA domain containing 5; *Ppox*, protoporphyrinogen oxidase; *Cfdp1*, craniofacial development protein 1; *Nptxr*, neuronal pentraxin receptor; *H6pd*, hexose-6-phosphate dehydrogenase/glucose 1-dehydrogenase; *Mrpl55*, mitochondrial ribosomal protein L55; *Sema3F*, semaphorin 3F, *SerpinE3*, serpin family E member 3; *Dpp7*, dipeptidyl peptidase 7; *Tmc06*, transmembrane and coiled-coil domains 6; *Cdc23*, cell division cycle 23; FaDu, hypopharyngeal cancer cells; SiHa, cervix cancer cells; HCT116, colon cancer cells; C26, colon cancer cells; LLC, Lewis lung carcinoma cells; pH6.5, pH6.5-exposed cancer cells; pH7.4, pH7.4-maintained cancer cells. *p < 0.05, **p < 0.01 ***p < 0.001, ****p < 0.0001.

stratified per BMI. Interestingly, plasma GUSB was increased only in cachectic patients with a usual BMI <20 kg/m^2 (Fig. S9k).

4. DISCUSSION

The contribution of host metabolism to tumoral growth is emerging and may reveal new therapeutic targets. For instance, the increased availability of fatty acids fosters triglyceride storage and lipid oxidation within cancer cells in parallel with their invasive potential [6,7]. Furthermore, proton accumulation in tumoral acidosis has been reported to promote lipolysis in cancer-associated adipocytes [10]. Therefore, we assumed that acidosis may also contribute to lipolysis at distance from the tumour, and this would occur through soluble secreted factors. For this reason, we exposed adipocytes to conditioned medium rather than performing co-cultures. This setting established that acid-exposed cancer cells sustain exogenous fatty acid craving by promoting subcutaneous and visceral adipocyte lipolysis. *In vivo*, tumoral acidosis was associated with distant adipose tissue depletion and induction of adipose lipolysis. Dampening tumoral acidosis with sodium bicarbonate buffer inhibited adipose tissue depletion, thereby demonstrating the causal link between tumoral acidosis and adipose tissue depletion *in vivo*. A transcriptomic

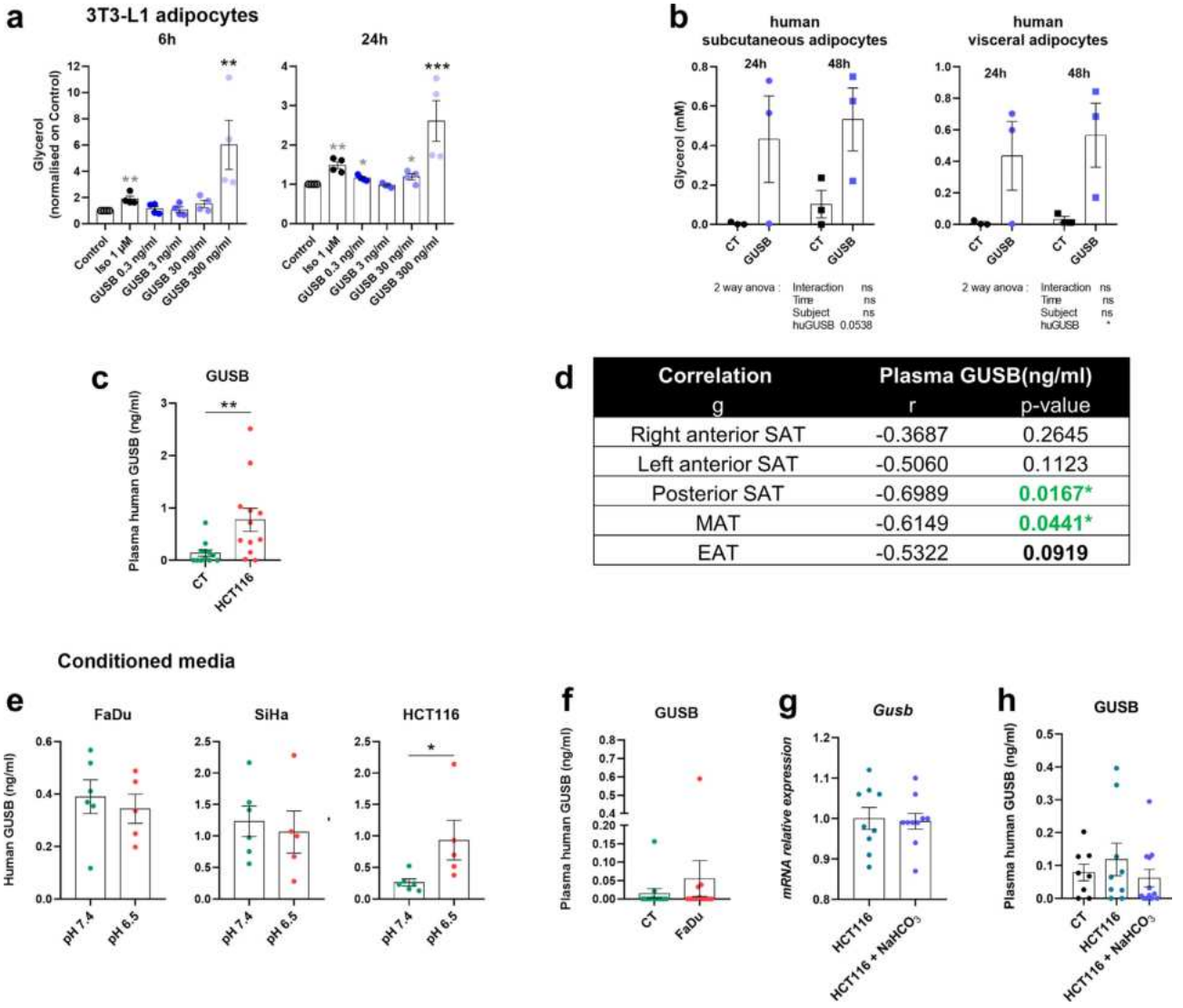

Figure 8: Human GUSB protein induces adipose lipolysis in murine and human adipocytes. (a) 3T3-L1 adipocytes (n = 4, each point corresponds to one n) treated with control medium without (control) or with 1 µM isoproterenol (Iso), or human recombinant GUSB at concentration of 0.3–300 ng/ml, for 6 h or 24 h. (b) Human primary subcutaneous and visceral adipocytes (n = 3, each point corresponds to one patient) treated with control medium (control) or 150 ng/ml human recombinant GUSB, for 24 h or 48 h. The results of the two-way ANOVA are shown below the graphs. (c) Plasma human GUSB protein concentration in male CT mice (sham-injected) and HCT116 tumour-bearing mice on day 16 post-injection (necropsy). (d) Correlation of right anterior, left anterior, posterior subcutaneous (SAT), visceral epididymal (EAT) and mesenteric (MAT) adipose tissue weights with plasma human GUSB concentrations, in HCT116 tumour-bearing mice, on the day of necropsy. In bold $p < 0.1$, in green bold $p < 0.05$. (e) Human GUSB protein concentration in conditioned media from human pH6.5/and pH7.4/FaDu, SiHa and HCT116 cancer cell lines (n = 5–6, each point corresponds to one n). (f) Human plasma protein GUSB concentrations in male FaDu tumour-bearing mice on the day of necropsy (n = 12). (g–h) *Gusb* expression in HCT116 tumour (g) and GUSB circulating levels (h) in HCT116-tumour bearing mice treated with $NaHCO_3$ (n = 8–12, each point corresponds to one n). FaDu, human hypopharyngeal cancer cells; SiHa, human cervix cancer cells; HCT116, human colon cancer cells; GUSB, glucuronidase beta. (c, e-f) Each point corresponds to one mouse. Data are presented as the mean ± SEM. *$p < 0.05$, **$p < 0.01$, ***$p < 0.001$. * shown in grey are t-test analysis results compared to the control condition.

approach comparing pH6.5-exposed and pH7.4-cultured cancer cells led us to pinpoint potential prolipolytic mediators, such as GUSB, which was able to induce lipolysis in mouse and human adipocytes. Altogether, we demonstrated that tumoral acidosis promotes adipose tissue lipolysis through the release of soluble prolipolytic factors such as GUSB.

Our transcriptomic analyses underline that pH6.5/cancer cells increase their import of fatty acids, which are either oxidised to fulfil their metabolic needs and/or stored in lipids droplets if present in excess. These results are in line with previous reports which used functional assays for these pathways [3—5,25,47].

The promotion of adipocyte lipolysis upon acidosis adaptation was observed in 5 of the 7 tested cell lines. PANC-1, a pancreatic ductal adenocarcinoma cell line, did not promote lipolysis upon acidosis adaptation, contrarily to MIA PaCa-2, another pancreatic ductal adenocarcinoma cell line. Compared to other pancreatic cancer cell lines, PANC-1 exhibits the most aggressive behaviour and the highest metabolic plasticity towards glucose, glutamine and fatty acid substrates [55,56]. Such high metabolic plasticity of pH6.5/PANC-1 cancer cells may underlie a lower fatty acid dependency, and thereby a lack of lipolysis induction upon acidosis adaptation in absence of fatty acids, as suggested by the similar consumption of glutamine and glucose in pH6.5/and pH7.4/PANC-1 cancer cells (Fig. S1g—h). In contrast, other pH6.5/cancer cells consumed less glutamine and glucose than pH7.4/cancer cells, in line with a higher dependency for fatty acids. pH6.5/C26 conditioned medium did not induce adipocyte lipolysis either. Intriguingly, we observed an important heterogeneity in the lipolytic response of primary adipocytes to pH6.5/C26 conditioned medium, with glycerol release correlating with the expression of fatty acid metabolism markers (*Plin2*, *Fabp4*) and prolipolytic factors (*Pthlh*, *Adm*). It suggests that this link between cancer fatty acid metabolism and adipocyte lipolysis induction is also present in C26. Of note, pH7.4/C26 conditioned medium was previously reported to be prolipolytic in 3T3-L1 adipocytes [57—59]. This apparent discrepancy may arise from the fact that we used a different model, namely primary adipocytes. It is currently unclear whether the ability for cancer cells to promote lipolysis upon acid adaptation translate systematically into pro-cachectic properties *in vivo*. One key element that underlies this translation would be the propensity of cancer cell lines to develop acidosis *in vivo* [60].

Here, we paid particular attention to the type of adipose tissue involved. SAT is the main fatty acid storage site because of its greater capacity for adipogenesis and lipogenesis than VAT with higher levels of stimulated lipolysis [61—63]. These differences are related to the distinct α- (antilipolytic) and β- (prolipolytic) adrenergic responses, as well as local inflammatory tone and insulin resistance [64]. In obesity, the differences are well described; SAT and VAT expansion respectively protect from or contribute to the metabolic alterations associated with obesity [65—67]. In cachexia, the differences between SAT and VAT were inconsistent from one study to another. The most described aspect so far is the inflammatory response with, in some studies, inflammation being more induced in the SAT than in the VAT upon cachexia [68,69], while other studies describe the opposite [70,71]. Besides, SAT and/or VAT depletion have been associated to a poor prognostic of survival with divergent results from one study to another in terms of which fat depot would be the most crucial [17,72—74]. In our study, pH6.5/conditioned medium promoted lipolysis of subcutaneous and visceral murine primary adipocytes to the same extent. In HCT116 tumour-bearing mice, we observed differences in lipolysis induction between fat depots. Adipose tissue lipolysis was more pronounced in left anterior SAT than in the right one. MAT seemed to be the most affected adipose tissue, with the highest increase in lipolysis enzymes. Interestingly, the weight of the two anterior SAT was associated with tumour weight, while the weight of the distant adipose tissues was associated primarily with tumoral acidosis. Consistent with these findings, the vicinity of the adipose tissue environment was demonstrated as a motor in the progression of tumour and metastasis [9,75]. Altogether, these results indicate that while the responsiveness of adipocytes to acid-exposed cancer cells is independent of their origin, lipolysis is not induced to the same extent in different fat depots *in vivo.* Close-to-the-tumour depots may be essential for tumour growth whereas distant tissues would release fatty acids in response to tumoral acidosis.

FaDu and HCT116 tumour-bearing models are consistently used as *in vivo* [48—53] and *in vitro* models [3,5,47] of tumoral acidosis. We selected pHLIP(var3) to detect acidosis as it is a reference method for this purpose [49,51,76,77]. Besides, pHLIP(var3) uptake and retention presented a direct correlation with tumour pH in HCT116 tumour-bearing mice [49]. Likewise, an accumulation of pHLIP(var3) demonstrate the spontaneous acidosis development in our HCT116 tumour-bearing mice.

Neutralisation of tumour acidosis with a systemic buffer is an approach that has already been used to identify mechanisms dependent on tumoral acidosis [1,48,78,79]. In line with previous reports, blood pH was not affected by $NaHCO_3$ administration in HCT116 tumour-bearing mice [78,79]. This systemic buffer must be administrated during the early stages of tumour growth to prevent tumour growth [78]. For this reason, our treatment began 4 days after HCT116 injection and not immediately after HCT116 injection. Neutralisation of acidosis with a sodium bicarbonate buffer highlights a new role for tumoral acidosis in tumour progression: the promotion of adipose tissue depletion at distance from the tumour. Despite previous report highlighting a neutralisation of tumoral acidosis in HCT116 tumour under $NaHCO_3$ treatment [48], the absence of functional measure of acidosis in our study constitutes a limitation. Unfortunately, sodium bicarbonate failed to reach its dose target in phase I/II clinical trials in patients with pancreatic cancer because of poor compliance due to unpleasant taste and/or gastrointestinal problems [80]. Other therapeutic approaches targeting tumoral acidosis, such as proton pump inhibitors (PPIs), have shown promising antitumour effects and are undergoing clinical evaluation [2]. As a more targeted approach, therapeutic agents guided by a pHLIP would allow to specifically inhibit the growth of cancer cells located in the acidic area [1,2,81].

Our transcriptomic approaches revealed that acid-exposed cancer cells exhibit increased expression of a panel of known, although unshared, prolipolytic factors. We also identified GUSB as a promising new key player in the promotion of adipose lipolysis. GUSB is a lysosomal glucuronidase enzyme that is involved in the breakdown of complex carbohydrates [82]. In hepatocellular carcinoma, GUSB has been reported to facilitate cancer cell proliferation, invasion, migration and resistance to anti-PDL1 agents [83]. To the best of our knowledge, GUSB has never been associated with cancer cachexia or adipocyte lipolysis. Here, we discovered that GUSB promotes lipolysis in both murine adipocyte cultures and primary human subcutaneous and visceral adipocytes.

We envisioned two hypotheses regarding the mechanisms by which GUSB fosters lipolysis. Firstly, GUSB can bind to the mannose-6-phosphate receptor [23,84,85], a receptor that can be bound as well by proliferin-1, described recently for its anti-adipogenesis and prolipolytic properties. However, this mechanism was not retained in the prolipolytic effect of proliferin-1 [23]. Secondly, lipolysis induction may arise from the enzymatic degradation of the extracellular 3T3-L1

adipocyte matrix by GUSB and the subsequent release of adipocyte inflammatory mediators [86]. However, the prolipolytic activity of GUSB observed in primary adipocytes, whose extracellular matrix was digested beforehand by collagenase, is not consistent with this hypothesis. Therefore, the mechanism by which GUSB induces lipolysis requires further investigation.

We speculate that the increased secretion of GUSB upon acidosis adaptation arises from increased lysosomal trafficking to the extracellular membrane. Indeed, in breast cancer, chronic acidosis was reported to drive the exocytosis of lysosomes and increase the secretion of degradation enzymes [54,87,88]. H^+-ATPases on lysosomal membranes contribute to lysosomal traffic, lysosomal acidification, and thereby acidification of the tumoral microenvironment during exocytosis. A difference in lysosomal trafficking between acid-exposed cancer cell lines may therefore explain why GUSB protein levels were increased in the conditioned medium of one out of the 3 cell lines despite an increase in its gene expression in the 3 cancer cell lines. Supporting this hypothesis, in parallel with the increased *Gusb* expression, genes associated with lysosomal transport were overexpressed in pH6.5/HCT116 cancer cells (Fig. S10). Extracellular release of GUSB is also dependent on its N-glycosylation profile [89,90] and the nature of the N-terminal and/or C-terminal peptides [91]. These features may also contribute to explain the difference in the GUSB secretion profile between the pH6.5/cancer cell lines.

Intriguingly, GUSB was correlated to adipose tissue depletion and increased in the HCT116 model. Of note, GUSB levels were not increased at the onset of fat mass loss, leading us to conclude that GUSB is not involved in the early phase of adipose tissue depletion and in the mitigating effect of bicarbonate on fat mass loss. This last observation underlines the existence of factors others than GUSB mediating the impact of tumoral acidosis on adipose tissue loss. Of note, cancer cachexia symptoms are thought to result from a combination of procachectic factors [33]. While GUSB can induce lipolysis *per se*, it is more probably a mix of prolipolytic mediators which promote the induction of *ex vivo* and *in vivo* lipolysis.

Our study indicates that GUSB is a novel prolipolytic mediator. Considering the differences between the *in vitro* and *in vivo* situations (e.g. acute versus chronic exposure, 'one-time' exposure versus the continuous exposure to factors that are regularly produced), we may speculate that while 150—300 ng/ml of GUSB is requested *in vitro* to observe a large induction of lipolysis, 1 ng/ml may be sufficient *in vivo* to elicit a physiological relevant prolipolytic effect. Future *in vivo* experiments with titrated doses of GUSB in healthy animals will help address this question. Futhermore, whether targeting GUSB is of therapeutic interest for cachexia-associated lipolysis in human cancer remains unclear. In patients with colorectal and lung cancer, GUSB levels did not differ between cachectic and non-cachectic patients. However, interestingly, GUSB was increased in cachectic patients compared to non-cachectic patients when considering only individuals with a low usual BMI. Unfortunately, the sample size is too low in this subset to draw any definitive conclusion about the role of GUSB in adipose tissue weight in this specific subtype of patients. If confirmed in a population with a larger sample size, GUSB may hold diagnostic or therapeutic potential, using approaches that inhibit GUSB [83], for this subset of patients. Plasma GUSB correlated positively with fat mass and BMI and negatively with lipolytic activity and body weight loss. These results are in line with those of another study showing a positive correlation between serum GUSB activity and BMI and total fat mass in pre/postmenopausal women [92]. GUSB gene expression is increased in the adipose tissue of genetically obese mice [93], and GUSB protein levels are increased in 3T3-L1 adipocytes treated with insulin or TNFα (used to induce insulin resistance) [94], raising the possibility of GUSB secretion by adipose tissues. The contribution of adipose tissue to plasma GUSB levels would explain the positive correlations between GUSB plasma levels and BMI and fat mass and may mask the tumoral contribution to GUSB levels in humans. This may also explain why GUSB is increased in cachectic versus non-cachectic patients only in those with a low usual BMI. We can further speculate that in patients with a higher BMI, which often goes with insulin resistance, GUSB production by the adipose tissue would be increased. Whether resistance to GUSB prolipolytic effect may arise in obesity as it is known for other adipokines needs to be investigated. However, these theories are not supported by the observation that in mice, a GUSB mutation, that leads to a disappearance of its activity, was associated to adipose tissue depletion [95]. More investigations are needed to fully unravel the pathophysiological role of GUSB. Key questions include whether GUSB can trigger adipose tissue weight loss in healthy animals and to which extent GUSB contributes to pathological weight loss in tumour-bearing animals.

Targeting the tumour microenvironment and its crosstalk with the host is emerging as a new cachexia treatment strategy [24]. Here, we pinpoint, for the first time, the role of tumoral acidosis in adipose tissue depletion associated with cancer cachexia. We highlight that acid-exposed cancer cells promote subcutaneous and visceral adipocyte lipolysis by releasing prolipolytic mediators. In this context, we identified GUSB as a new prolipolytic mediator, the underlying mechanisms of which requires further investigation. Two main prospects arise from our work. The first is the potential of tumoral acidosis as a prognostic marker of adipose tissue depletion associated with cancer. Early prognostic markers are of crucial importance for tackling cachexia in a personalized and efficient manner [24]. The second is the anti-cachectic potential of approaches targeting tumoral acidosis such as pHLIP-guided therapeutic agents. Such concept paves the way for dualistic approaches tackling both metastasis formation and cachexia, two key determinants of cancer mortality.

FUNDING SOURCES

This work was funded by the FSR (Action de Recherche Concertée (ARC) LIPOCAN, 19—24.096) and the Télévie (7.4511.21). LBB is a Collen-Francqui Research Professor and grateful for the support of the Francqui Fondation. LBB is the recipient of subsidies from the Walloon Region in the context of the funding of the strategic axis FRFS-WELBIO (40009849), as well as the Fonds Wetenschappelijk Onderzoek - Vlaanderen (FWO) and the Fonds de la Recherche Scientifique FNRS under EOS Project No. 40007505. CL is a postdoctoral fellow from the Télévie (7.4511.21). MMT is a postdoctoral fellow from the Fonds de la Recherche Scientifique (FRS)-FNRS. NMD is a recipient of grants from the FRS-FNRS (PINT-MULTI R.8013.19 (NEURON, call 2019) and PDR T.0068.19).

CREDIT AUTHORSHIP CONTRIBUTION STATEMENT

Camille Lefevre: Writing — review & editing, Writing — original draft, Visualization, Validation, Methodology, Investigation, Formal analysis, Data curation, Conceptualization. **Morgane M. Thibaut:** Formal analysis, Writing — review & editing. **Audrey Loumaye:** Investigation, Writing — review & editing. **Jean-Paul Thissen:** Investigation, Writing — review & editing. **Audrey M. Neyrinck:** Resources, Writing — review & editing. **Benoit Navez:** Investigation, Writing — review & editing. **Nathalie M. Delzenne:** Resources, Writing — review & editing. **Olivier Feron:** Conceptualization, Methodology, Resources, Writing —

review & editing. **Laure B. Bindels:** Conceptualization, Funding acquisition, Methodology, Project administration, Resources, Supervision, Validation, Writing — original draft, Writing — review & editing.

ACKNOWLEDGEMENTS

We thank Bouazza Es Saadi, Stéphanie Delieux, Marine Olivier, Amélie Flandin and Martin Nicolas for their skilled technical assistance. We also thank Dr Lionel Mignon, Inès Monchaux, Dr Alexandra Degraeve, Sophie Lecop and Dr Adeline Dolly for their help during mouse experiments. We thank Dr Julie Vanacker and Marie de Barsy for their help with the clinical study. We thank Dr Maximilien Thoma, Dr Yannick Deswysen, Dr Lancelot Marique and Rita Maria Trindade Almeida for their help in the patient's recruitment. We are grateful to Dr Caroline Bouzin and the IREC Imaging Platform (2IP) for their assistance with histological analyses.

DECLARATION OF COMPETING INTEREST

The authors declare that they have no known competing financial interests or personal relationships that could have appeared to influence the work reported in this paper.

DATA AVAILABILITY

Raw RNA sequences can be found in the Gene Expression Omnibus (GEO) database (project ID: GSE253054). Additional raw data will be made available upon request.

APPENDIX A. SUPPLEMENTARY DATA

Supplementary data to this article can be found online at https://doi.org/10.1016/j.molmet.2024.101930.

REFERENCES

[1] Corbet C, Feron O. Tumour acidosis: from the passenger to the driver's seat. Nat Rev Cancer 2017;17(10):577—93. https://doi.org/10.1038/nrc.2017.77.

[2] Pillai SR, Damaghi M, Marunaka Y, Spugnini EP, Fais S, Gillies RJ. Causes, consequences, and therapy of tumors acidosis. Cancer Metastasis Rev 2019;38(1—2):205—22. https://doi.org/10.1007/s10555-019-09792-7.

[3] Corbet C, Pinto A, Martherus R, Santiago de Jesus JP, Polet F, Feron O. Acidosis drives the reprogramming of fatty acid metabolism in cancer cells through changes in mitochondrial and histone acetylation. Cell Metabol 2016;24(2):311—23. https://doi.org/10.1016/j.cmet.2016.07.003.

[4] Rolver MG, Holland LKK, Ponniah M, Prasad NS, Yao J, Schnipper J, et al. Chronic acidosis rewires cancer cell metabolism through PPARα signaling. Int J Cancer 2023;152(8):1668—84. https://doi.org/10.1002/ijc.34404.

[5] Corbet C, Bastien E, Santiago de Jesus JP, Dierge E, Martherus R, Vander Linden C, et al. TGFβ2-induced formation of lipid droplets supports acidosis-driven EMT and the metastatic spreading of cancer cells. Nat Commun 2020;11. https://doi.org/10.1038/s41467-019-14262-3.

[6] Koundouros N, Poulogiannis G. Reprogramming of fatty acid metabolism in cancer. Br J Cancer 2020;122(1):4—22. https://doi.org/10.1038/s41416-019-0650-z.

[7] Balaban S, Shearer RF, Lee LS, van Geldermalsen M, Schreuder M, Shtein HC, et al. Adipocyte lipolysis links obesity to breast cancer growth: adipocyte-derived fatty acids drive breast cancer cell proliferation and migration. Cancer Metabol 2017;5. https://doi.org/10.1186/s40170-016-0163-7.

[8] Rybinska I, Agresti R, Trapani A, Tagliabue E, Triulzi T. Adipocytes in breast cancer, the thick and the thin. Cells 2020;9(3). https://doi.org/10.3390/cells9030560.

[9] Nieman KM, Kenny HA, Penicka CV, Ladanyi A, Buell-Gutbrod R, Zillhardt MR, et al. Adipocytes promote ovarian cancer metastasis and provide energy for rapid tumor growth. Nat Med 2011;17(11):1498—503. https://doi.org/10.1038/nm.2492.

[10] Cremer J, Brohée L, Dupont L, Lefevre C, Peiffer R, Saarinen AM, et al. Acidosis-induced regulation of adipocyte G0S2 promotes crosstalk between adipocytes and breast cancer cells as well as tumor progression. Cancer Lett 2023;569:216306. https://doi.org/10.1016/j.canlet.2023.216306.

[11] Sun X, Feng X, Wu X, Lu Y, Chen K, Ye Y. Fat wasting is damaging: role of adipose tissue in cancer-associated cachexia. Front Cell Dev Biol 2020;8. https://doi.org/10.3389/fcell.2020.00033.

[12] Baracos VE, Martin L, Korc M, Guttridge DC, Fearon KCH. Cancer-associated cachexia. Nat Rev Dis Prim 2018;4(1):1—18. https://doi.org/10.1038/nrdp.2017.105.

[13] Ferrara M, Samaden M, Ruggieri E, Vénéreau E. Cancer cachexia as a multiorgan failure: reconstruction of the crime scene. Front Cell Dev Biol 2022;10.

[14] Fouladiun M, Körner U, Bosaeus I, Daneryd P, Hyltander A, Lundholm KG. Body composition and time course changes in regional distribution of fat and lean tissue in unselected cancer patients on palliative care–correlations with food intake, metabolism, exercise capacity, and hormones. Cancer 2005;103(10):2189—98. https://doi.org/10.1002/cncr.21013.

[15] Tsoli M, Swarbrick MM, Robertson GR. Lipolytic and thermogenic depletion of adipose tissue in cancer cachexia. Semin Cell Dev Biol 2016;54:68—81. https://doi.org/10.1016/j.semcdb.2015.10.039.

[16] Das SK, Eder S, Schauer S, Diwoky C, Temmel H, Guertl B, et al. Adipose triglyceride lipase contributes to cancer-associated cachexia. Science (New York, N.Y.) 2011;333(6039):233—8. https://doi.org/10.1126/science.1198973.

[17] Kays JK, Shahda S, Stanley M, Bell TM, O'Neill BH, Kohli MD, et al. Three cachexia phenotypes and the impact of fat-only loss on survival in FOLFIRINOX therapy for pancreatic cancer. Journal of Cachexia, Sarcopenia and Muscle 2018;9(4):673—84. https://doi.org/10.1002/jcsm.12307.

[18] Grabner GF, Xie H, Schweiger M, Zechner R. Lipolysis: cellular mechanisms for lipid mobilization from fat stores. Nat Metab 2021;3(11):1445—65. https://doi.org/10.1038/s42255-021-00493-6.

[19] Weber BZC, Arabaci DH, Kir S. Metabolic reprogramming in adipose tissue during cancer cachexia. Front Oncol 2022;12:848394. https://doi.org/10.3389/fonc.2022.848394.

[20] Agustsson T, Rydén M, Hoffstedt J, van Harmelen V, Dicker A, Laurencikiene J, et al. Mechanism of increased lipolysis in cancer cachexia. Cancer Res 2007;67(11):5531—7. https://doi.org/10.1158/0008-5472.CAN-06-4585.

[21] Tsoli M, Schweiger M, Vanniasinghe AS, Painter A, Zechner R, Clarke S, et al. Depletion of white adipose tissue in cancer cachexia syndrome is associated with inflammatory signaling and disrupted circadian regulation. PLoS One 2014;9(3):e92966. https://doi.org/10.1371/journal.pone.0092966.

[22] Rohm M, Schäfer M, Laurent V, Üstünel BE, Niopek K, Algire C, et al. An AMP-activated protein kinase—stabilizing peptide ameliorates adipose tissue wasting in cancer cachexia in mice. Nat Med 2016;22(10):14.

[23] Nguyen TD, Miyatake Y, Yoshida T, Kawahara H, Hanayama R. Tumor-secreted proliferin-1 regulates adipogenesis and lipolysis in cachexia. Int J Cancer 2020. https://doi.org/10.1002/ijc.33418.

[24] Argilés JM, López-Soriano FJ, Stemmler B, Busquets S. Cancer-associated cachexia — understanding the tumour macroenvironment and microenvironment to improve management. Nat Rev Clin Oncol 2023;20(4):250—64. https://doi.org/10.1038/s41571-023-00734-5.

[25] Corbet C, Draoui N, Polet F, Pinto A, Drozak X, Riant O, et al. The SIRT1/HIF2α Axis drives reductive glutamine metabolism under chronic acidosis and alters

tumor response to therapy. Cancer Res 2014;74(19):5507–19. https://doi.org/10.1158/0008-5472.CAN-14-0705.

[26] Weerakkody D, Moshnikova A, Thakur MS, Moshnikova V, Daniels J, Engelman DM, et al. Family of pH (low) insertion peptides for tumor targeting. Proc Natl Acad Sci USA 2013;110(15):5834–9. https://doi.org/10.1073/pnas.1303708110.

[27] Thibaut MM, Sboarina M, Roumain M, Pötgens SA, Neyrinck AM, Destrée F, et al. Inflammation-induced cholestasis in cancer cachexia. Journal of Cachexia, Sarcopenia and Muscle 2021;12(1):70–90. https://doi.org/10.1002/jcsm.12652.

[28] Bolger AM, Lohse M, Usadel B. Trimmomatic: a flexible trimmer for Illumina sequence data. Bioinformatics 2014;30(15):2114–20. https://doi.org/10.1093/bioinformatics/btu170.

[29] Dobin A, Davis CA, Schlesinger F, Drenkow J, Zaleski C, Jha S, et al. STAR: ultrafast universal RNA-seq aligner. Bioinformatics 2013;29(1):15–21. https://doi.org/10.1093/bioinformatics/bts635.

[30] Lawrence M, Huber W, Pagès H, Aboyoun P, Carlson M, Gentleman R, et al. Software for computing and annotating genomic ranges. PLoS Comput Biol 2013;9(8):e1003118. https://doi.org/10.1371/journal.pcbi.1003118.

[31] Love MI, Huber W, Anders S. Moderated estimation of fold change and dispersion for RNA-seq data with DESeq2. Genome Biol 2014;15(12):550. https://doi.org/10.1186/s13059-014-0550-8.

[32] Uhlén M, Karlsson MJ, Hober A, Svensson AS, Scheffel J, Kotol D, et al. The human secretome. Sci Signal. 2019;12(609):eaaz0274. https://doi.org/10.1126/scisignal.aaz0274.

[33] Freire PP, Fernandez GJ, de Moraes D, Cury SS, Pai-Silva MD, Reis PP dos, et al. The expression landscape of cachexia-inducing factors in human cancers. Journal of Cachexia, Sarcopenia and Muscle 2020;11(4):947–61. https://doi.org/10.1002/jcsm.12565.

[34] Uhlén M, Fagerberg L, Hallström BM, Lindskog C, Oksvold P, Mardinoglu A, et al. Tissue-based map of the human proteome. Science 2015;347(6220):1260419. https://doi.org/10.1126/science.1260419.

[35] Rohart F, Gautier B, Singh A, Cao K-AL. mixOmics: an R package for 'omics feature selection and multiple data integration. PLoS Comput Biol 2017;13(11):e1005752. https://doi.org/10.1371/journal.pcbi.1005752.

[36] Yu G, Wang L-G, Han Y, He Q-Y. clusterProfiler: an R Package for comparing biological themes among gene clusters. OMICS A J Integr Biol 2012;16(5):284–7. https://doi.org/10.1089/omi.2011.0118.

[37] Korotkevich G, Sukhov V, Budin N, Shpak B, Artyomov MN, Sergushichev A. Fast gene set enrichment analysis: 060012. 2021. https://doi.org/10.1101/060012.

[38] Young MD, Wakefield MJ, Smyth GK, Oshlack A. Gene ontology analysis for RNA-seq: accounting for selection bias. Genome Biol 2010;11(2):R14. https://doi.org/10.1186/gb-2010-11-2-r14.

[39] Vandesompele J, De Preter K, Pattyn F, Poppe B, Van Roy N, De Paepe A, et al. Accurate normalization of real-time quantitative RT-PCR data by geometric averaging of multiple internal control genes. Genome Biol 2002;3(7). https://doi.org/10.1186/gb-2002-3-7-research0034. research0034.1.

[40] Loumaye A, de Barsy M, Nachit M, Lause P, Frateur L, van Maanen A, et al. Role of Activin A and myostatin in human cancer cachexia. J Clin Endocrinol Metabol 2015;100(5):2030–8. https://doi.org/10.1210/jc.2014-4318.

[41] Fearon K, Strasser F, Anker SD, Bosaeus I, Bruera E, Fainsinger RL, et al. Definition and classification of cancer cachexia: an international consensus. Lancet Oncol 2011;12(5):489–95. https://doi.org/10.1016/S1470-2045(10)70218-7.

[42] Fox J, Weisberg S. An R companion to applied regression. SAGE; 2018.

[43] Bates D, Mächler M, Bolker B, Walker S. Fitting linear mixed-effects models using lme4. J Stat Software 2015;67:1–48. https://doi.org/10.18637/jss.v067.i01.

[44] Lenth RV. Least-squares means: the R package lsmeans. J Stat Software 2016;69:1–33. https://doi.org/10.18637/jss.v069.i01.

[45] Okuro K, Fukuhara A, Minemura T, Hayakawa T, Nishitani S, Okuno Y, et al. Glutamine deficiency induces lipolysis in adipocytes. Biochem Biophys Res Commun 2021;585:155–61. https://doi.org/10.1016/j.bbrc.2021.11.043.

[46] Naito C, Okada K. Effect of glucose on lipolysis and on release of lipolytic products in isolated adipocytes. American Journal of Physiology-Legacy Content 1975;228(1):92–7. https://doi.org/10.1152/ajplegacy.1975.228.1.92.

[47] Dierge E, Debock E, Guilbaud C, Corbet C, Mignolet E, Mignard L, et al. Peroxidation of n-3 and n-6 polyunsaturated fatty acids in the acidic tumor environment leads to ferroptosis-mediated anticancer effects. Cell Metabol 2021. https://doi.org/10.1016/j.cmet.2021.05.016.

[48] Estrella V, Chen T, Lloyd M, Wojtkowiak J, Cornnell HH, Ibrahim-Hashim A, et al. Acidity generated by the tumor microenvironment drives local invasion. Cancer Res 2013;73(5):1524–35. https://doi.org/10.1158/0008-5472.CAN-12-2796.

[49] Tapmeier TT, Moshnikova A, Beech J, Allen D, Kinchesh P, Smart S, et al. The pH low insertion peptide pHLIP Variant 3 as a novel marker of acidic malignant lesions. Proc Natl Acad Sci USA 2015;112(31):9710–5. https://doi.org/10.1073/pnas.1509488112.

[50] Ray KJ, Simard MA, Larkin JR, Coates J, Kinchesh P, Smart SC, et al. Tumor pH and protein concentration contribute to the signal of amide proton transfer magnetic resonance imaging. Cancer Res 2019;79(7):1343–52. https://doi.org/10.1158/0008-5472.CAN-18-2168.

[51] Huang G, Zhao T, Wang C, Nham K, Xiong Y, Gao X, et al. PET imaging of occult tumours by temporal integration of tumour-acidosis signals from pH-sensitive 64Cu-labelled polymers. Nat Biomed Eng 2019;4(3):314–24. https://doi.org/10.1038/s41551-019-0416-1.

[52] Zhao T, Huang G, Li Y, Yang S, Ramezani S, Lin Z, et al. A transistor-like pH nanoprobe for tumour detection and image-guided surgery. Nat Biomed Eng 2016;1. https://doi.org/10.1038/s41551-016-0006. 0006.

[53] Lee S-H, McIntyre D, Honess D, Hulikova A, Pacheco-Torres J, Cerdán S, et al. Carbonic anhydrase IX is a pH-stat that sets an acidic tumour extracellular pH in vivo. Br J Cancer 2018;119(5):622–30. https://doi.org/10.1038/s41416-018-0216-5.

[54] Damaghi M, Tafreshi NK, Lloyd MC, Sprung R, Estrella V, Wojtkowiak JW, et al. Chronic acidosis in the tumour microenvironment selects for overexpression of LAMP2 in the plasma membrane. Nat Commun 2015;6(1):8752. https://doi.org/10.1038/ncomms9752.

[55] Novák Š, Kolář M, Szabó A, Vernerová Z, Lacina L, Strnad H, et al. Desmoplastic crosstalk in pancreatic ductal adenocarcinoma is reflected by different responses of panc-1, MIAPaCa-2, PaTu-8902, and CAPAN-2 cell lines to cancer-associated/normal fibroblasts. Cancer Genomics Proteomics 2021;18(3):221–43. https://doi.org/10.21873/cgp.20254.

[56] Masoud R, Reyes-Castellanos G, Lac S, Garcia J, Dou S, Shintu L, et al. Targeting mitochondrial complex I overcomes chemoresistance in high OXPHOS pancreatic cancer. Cell Reports Medicine 2020;1(8). https://doi.org/10.1016/j.xcrm.2020.100143.

[57] Chitti SV, Kang T, Fonseka P, Marzan AL, Stewart S, Shahi S, et al. Proteomic analysis of the small extracellular vesicles and soluble secretory proteins from cachexia inducing and non-inducing cancer cells. Proteomics 2023;23(15):2100314. https://doi.org/10.1002/pmic.202100314.

[58] Xiong H, Ye J, Xie K, Hu W, Xu N, Yang H. Exosomal IL-8 derived from Lung Cancer and Colon Cancer cells induced adipocyte atrophy via NF-κB signaling pathway. Lipids Health Dis 2022;21:147. https://doi.org/10.1186/s12944-022-01755-2.

[59] Ji H, Englmaier F, Morigny P, Giroud M, Gräsle P, Brings S, et al. Development of a peptide drug restoring AMPK and adipose tissue functionality in cancer cachexia. Mol Ther: The Journal of the American Society of Gene Therapy 2023;31(8):2408–21. https://doi.org/10.1016/j.ymthe.2023.06.020.

[60] Boedtkjer E, Pedersen SF. The acidic tumor microenvironment as a driver of cancer. Annu Rev Physiol 2020;82(1):103–26. https://doi.org/10.1146/annurev-physiol-021119-034627.

[61] Arner P, Langin D. Lipolysis in lipid turnover, cancer cachexia, and obesity-induced insulin resistance. Trends Endocrinol Metabol 2014;25(5):255–62. https://doi.org/10.1016/j.tem.2014.03.002.

[62] Sztalryd C, Kraemer FB. Differences in hormone-sensitive lipase expression in white adipose tissue from various anatomic locations of the rat. Metab, Clin Exp 1994;43(2):241–7. https://doi.org/10.1016/0026-0495(94)90252-6.

[63] Virtue S, Vidal-Puig A. Adipose tissue expandability, lipotoxicity and the Metabolic Syndrome–an allostatic perspective. Biochim Biophys Acta 2010;1801(3):338–49. https://doi.org/10.1016/j.bbalip.2009.12.006.

[64] Ibrahim MM. Subcutaneous and visceral adipose tissue: structural and functional differences. Obes Rev 2010;11(1):11–8. https://doi.org/10.1111/j.1467-789X.2009.00623.x.

[65] Després J-P, Lemieux I. Abdominal obesity and metabolic syndrome. Nature 2006;444(7121):881–7. https://doi.org/10.1038/nature05488.

[66] Satoor SN, Puranik AS, Kumar S, Williams MD, Ghale M, Rahalkar A, et al. Location, location, location: beneficial effects of autologous fat transplantation. Sci Rep 2011;1. https://doi.org/10.1038/srep00081.

[67] Lee M-J, Wu Y, Fried SK. Adipose tissue heterogeneity: implication of depot differences in adipose tissue for obesity complications. Mol Aspect Med 2013;34(1):1–11. https://doi.org/10.1016/j.mam.2012.10.001.

[68] Batista ML, Olivan M, Alcantara PSM, Sandoval R, Peres SB, Neves RX, et al. Adipose tissue-derived factors as potential biomarkers in cachectic cancer patients. Cytokine 2013;61(2):532–9. https://doi.org/10.1016/j.cyto.2012.10.023.

[69] Molfino A, Carletti R, Imbimbo G, Amabile MI, Belli R, di Gioia CRT, et al. Histomorphological and inflammatory changes of white adipose tissue in gastrointestinal cancer patients with and without cachexia. Journal of Cachexia, Sarcopenia and Muscle 2022;13(1):333–42. https://doi.org/10.1002/jcsm.12893.

[70] Miller J, Dreczkowski G, Ramage MI, Wigmore SJ, Gallagher IJ, Skipworth RJE. Adipose depot gene expression and intelectin-1 in the metabolic response to cancer and cachexia. Journal of Cachexia, Sarcopenia and Muscle 2020;11(4):1141–53. https://doi.org/10.1002/jcsm.12568.

[71] Han J, Wang Y, Qiu Y, Sun D, Liu Y, Li Z, et al. Single-cell sequencing unveils key contributions of immune cell populations in cancer-associated adipose wasting. Cell Discovery 2022;8(1):1–22. https://doi.org/10.1038/s41421-022-00466-3.

[72] Ebadi M, Martin L, Ghosh S, Field CJ, Lehner R, Baracos VE, et al. Subcutaneous adiposity is an independent predictor of mortality in cancer patients. Br J Cancer 2017;117(1):148–55. https://doi.org/10.1038/bjc.2017.149.

[73] Chung E, Lee HS, Cho E-S, Park EJ, Baik SH, Lee KY, et al. Changes in body composition during adjuvant FOLFOX chemotherapy and overall survival in non-metastatic colon cancer. Cancers 2019;12(1):60. https://doi.org/10.3390/cancers12010060.

[74] Al-Sawaf O, Weiss J, Skrzypski M, Lam JM, Karasaki T, Zambrana F, et al. Body composition and lung cancer-associated cachexia in TRACERx. Nat Med 2023;29(4):846–58. https://doi.org/10.1038/s41591-023-02232-8.

[75] Nieman KM, Romero IL, Van Houten B, Lengyel E. Adipose tissue and adipocytes supports tumorigenesis and metastasis. Biochim Biophys Acta 2013;1831(10):1533–41. https://doi.org/10.1016/j.bbalip.2013.02.010.

[76] Wyatt LC, Lewis JS, Andreev OA, Reshetnyak YK, Engelman DM. Applications of pHLIP Technology for cancer imaging and therapy. Trends Biotechnol 2017;35(7):653–64. https://doi.org/10.1016/j.tibtech.2017.03.014.

[77] Anemone A, Consolino L, Arena F, Capozza M, Longo DL. Imaging tumor acidosis: a survey of the available techniques for mapping in vivo tumor pH. Cancer Metastasis Rev 2019;38(1):25–49. https://doi.org/10.1007/s10555-019-09782-9.

[78] Ibrahim-Hashim A, Cornnell HH, Abrahams D, Lloyd M, Bui M, Gillies RJ, et al. Systemic buffers inhibit carcinogenesis in TRAMP mice. J Urol 2012;188(2):624–31. https://doi.org/10.1016/j.juro.2012.03.113.

[79] Robey IF, Baggett BK, Kirkpatrick ND, Roe DJ, Dosescu J, Sloane BF, et al. Bicarbonate increases tumor pH and inhibits spontaneous metastases. Cancer Res 2009;69(6):2260–8. https://doi.org/10.1158/0008-5472.CAN-07-5575.

[80] Gillies RJ, Ibrahim-Hashim A, Ordway B, Gatenby RA. Back to basic: trials and tribulations of alkalizing agents in cancer. Front Oncol 2022;12:981718. https://doi.org/10.3389/fonc.2022.981718.

[81] Deskeuvre M, Lan J, Dierge E, Messens J, Riant O, Corbet C, et al. Targeting cancer cells in acidosis with conjugates between the carnitine palmitoyltransferase 1 inhibitor etomoxir and pH (low) insertion peptides. Int J Pharm 2022;624:122041. https://doi.org/10.1016/j.ijpharm.2022.122041.

[82] Vogler C, Galvin N, Levy B, Grubb J, Jiang J, Zhou XY, et al. Transgene produces massive overexpression of human β-glucuronidase in mice, lysosomal storage of enzyme, and strain-dependent tumors. Proc Natl Acad Sci USA 2003;100(5):2669–73. https://doi.org/10.1073/pnas.0437941100.

[83] Kong X, Zheng Z, Song G, Zhang Z, Liu H, Kang J, et al. Over-expression of GUSB leads to primary resistance of anti-PD1 therapy in hepatocellular carcinoma. Front Immunol 2022;13.

[84] Urayama A, Grubb JH, Sly WS, Banks WA. Mannose 6-phosphate receptor–mediated transport of sulfamidase across the blood–brain barrier in the newborn mouse. Mol Ther : The Journal of the American Society of Gene Therapy 2008;16(7):1261–6. https://doi.org/10.1038/mt.2008.84.

[85] Sleat DE, Zheng H, Qian M, Lobel P. Identification of sites of mannose 6-phosphorylation on lysosomal proteins. Mol Cell Proteomics 2006;5(4):686–701. https://doi.org/10.1074/mcp.M500343-MCP200.

[86] Triggiani M, Granata F, Oriente A, De Marino V, Gentile M, Calabrese C, et al. Secretory phospholipases A2 induce β-glucuronidase release and IL-6 production from human lung Macrophages1. J Immunol 2000;164(9):4908–15. https://doi.org/10.4049/jimmunol.164.9.4908.

[87] Damaghi M, Gillies R. Phenotypic changes of acid-adapted cancer cells push them toward aggressiveness in their evolution in the tumor microenvironment. Cell Cycle 2017;16(19):1739–43. https://doi.org/10.1080/15384101.2016.1231284.

[88] Glunde K, Guggino SE, Solaiyappan M, Pathak AP, Ichikawa Y, Bhujwalla ZM. Extracellular acidification alters lysosomal trafficking in human breast cancer cells. Neoplasia 2003;5(6):533–45.

[89] Mori D, Shibata K, Yamasaki S. C-type lectin receptor dectin-2 binds to an endogenous protein β-glucuronidase on dendritic cells. PLoS One 2017;12(1):e0169562. https://doi.org/10.1371/journal.pone.0169562.

[90] Shipley JM, Grubb JH, Sly WS. The role of glycosylation and phosphorylation in the expression of active human beta-glucuronidase. J Biol Chem 1993;268(16):12193–8. https://doi.org/10.1016/S0021-9258(19)50325-8.

[91] Elliger SS, Elliger CA, Lang C, Watson GL. Enhanced secretion and uptake of β-glucuronidase improves adeno-associated viral-mediated gene therapy of mucopolysaccharidosis type VII mice. Mol Ther 2002;5(5):617–26. https://doi.org/10.1006/mthe.2002.0594.

[92] Funk JL, Wertheim BC, Frye JB, Blew RM, Nicholas JS, Chen Z, et al. Association of ß-glucuronidase activity with menopausal status, ethnicity, adiposity, and inflammation in women. Menopause 2023;30(2):186. https://doi.org/10.1097/GME.0000000000002106.

[93] van Eijk M, Aten J, Bijl N, Ottenhoff R, van Roomen CPAA, Dubbelhuis PF, et al. Reducing glycosphingolipid content in adipose tissue of obese mice restores insulin sensitivity, adipogenesis and reduces inflammation. PLoS One 2009;4(3):e4723. https://doi.org/10.1371/journal.pone.0004723.

[94] Chan H, Bhide KP, Vaidyam A, Hedrick V, Sobreira TJP, Sors TG, et al. Proteomic analysis of 3T3-L1 adipocytes treated with insulin and TNF-α. Proteomes 2019;7(4):35. https://doi.org/10.3390/proteomes7040035.

[95] Woloszynek JC, Coleman T, Semenkovich CF, Sands MS. Lysosomal dysfunction results in altered energy balance. J Biol Chem 2007;282(49):35765–71. https://doi.org/10.1074/jbc.M705124200.

